Stapp Car Crash Journal, Vol. 58 (November 2014), pp.
Copyright © 2014 The Stapp Association

Validation of an "Intelligent Mouthguard" single event head impact dosimeter

Adam Bartsch, Sergey Samorezov, Edward Benzel
Cleveland Clinic

Vincent Miele
University of Pittsburgh, Cleveland Clinic

Daniel Brett
Sportsguard Laboratories Inc.

ABSTRACT – Dating to Colonel John Paul Stapp MD in 1975, scientists have desired to measure live human head impacts with accuracy and precision. But no instrument exists to accurately and precisely quantify single head impact events. Our goal is to develop a practical single event head impact dosimeter known as "Intelligent Mouthguard" and quantify its performance on the benchtop, in vitro and in vivo.

In the Intelligent Mouthguard hardware, limited gyroscope bandwidth requires an algorithm-based correction as a function of impact duration. After we apply gyroscope correction algorithm, Intelligent Mouthguard results at time of CG linear acceleration peak correlate to the Reference Hybrid III within our tested range of pulse durations and impact acceleration profiles in American football and Boxing in vitro tests: American football, IMG=1.00REF-1.1g, R^2=0.99; maximum time of peak XYZ component imprecision 3.6g and 370rad/s^2; maximum time of peak azimuth and elevation imprecision 4.8° and 2.9°; maximum average XYZ component temporal imprecision 3.3g and 390rad/s^2. Boxing, IMG=1.00REF-0.9g, R^2=0.99, R^2=0.98; maximum time of peak XYZ component imprecision 3.9g and 390rad/s^2, maximum time of peak azimuth and elevation imprecision 2.9° and 2.1°; average XYZ component temporal imprecision 4.0g and 440rad/s^2. In vivo Intelligent Mouthguard true positive head impacts from American football players and amateur boxers have temporal characteristics (first harmonic frequency from 35Hz to 79Hz) within our tested benchtop (first harmonic frequency <180Hz) and in vitro (first harmonic frequency <100Hz) ranges.

Our conclusions apply only to situations where the rigid body assumption is valid, sensor-skull coupling is maintained and the ranges of tested parameters and harmonics fall within the boundaries of harmonics validated in vitro. For these situations, Intelligent Mouthguard qualifies as a single event dosimeter in American football and Boxing.

KEYWORDS – Concussion, Mild Traumatic Brain Injury, Intelligent Mouthguard, Single Event Head Impact Dosimeter, mTBI

INTRODUCTION

Approximately 173,000 persons under 19 years old are treated in emergency departments for non-fatal sport and recreation traumatic brain injury and concussion annually in the US (Centers for Disease Control, 2011) and 85% of all military mild traumatic brain injuries occur during non-deployment activities (Institute of Medicine and National Research Council, 2014).

Address correspondence to Adam Bartsch PhD PE, Cleveland Clinic, 1730 West 25th Street LUTH 2-C, Cleveland, OH 44113. Electronic mail: bartsca@ccf.org

Concussion and long-term brain injury is a function of single and cumulative head impact dose; e.g. a function of kinematics transferred to the rigid skull, then brain, during an impact. The Institute of Medicine recently reported there are currently inadequate data to define the multi-parameter impact dose thresholds for concussions in youth (Institute of Medicine and National Research Council, 2014).

Multi-parameter impact dose thresholds cannot be developed until an accurate and precise single event dosimeter is created. Unfortunately, there is no accurate and precise single event dosimeter available. Lacking a single event dosimeter, frontline caregivers continue to rely on subjective identification of at-risk

athletes, often missing concussions (Mansell et al., 2010) with approximately 50% of concussed athletes unidentified (McCrea et al., 2004). Undiagnosed concussion increases lost time from school (Arbogast et al., 2013) and risk of death due to Second Impact Syndrome (Cantu, 1998). Sub-concussive impact accumulation carries risks for depression (Guskiewicz et al., 2007a), suicide (Omalu et al., 2010), cognitive decline (Guskiewicz et al., 2005), Chronic Traumatic Encephalopathy (CTE) (Omalu et al., 2005; McKee et al., 2009), dementia (Jordan, 2000), Alzheimer's (Plassman et al., 2000) and Parkinson's (Daneshvar et al., 2011) Diseases.

Single event head impact doses provide valuable human head impact tolerance data to supplement existing human cadaver testing. Colonel John Paul Stapp advocated for this in 1975 (Stapp, 1978) when he "…*recommended instrumenting (American) football players and boxers… when subminiature instrumentation began to be developed*." Instrumenting humans in impact-rich environments fosters objective concussive and sub-concussive injury criteria to supplement the cadaver-based Head Injury Criterion. Dr. James McElhaney, at the 2005 Stapp Car Crash Conference (McElhaney, 2005), underscored the need for additional head injury criteria that "… *correlate with the broad spectrum of skull and brain injury mechanisms.*" Dr. McElhaney further advocated for using real-world doses in finite element models to "*accurately predict the extent and location of the damaged areas of the brain to assist neurological diagnoses, crashworthiness design and helmet design.*" Finally, Duma and Rowson (Duma and Rowson, 2011) endorsed multi-factorial spatial and temporal characterization of concussive impacts by stating "…*concussion is a result of linear head acceleration, rotational head acceleration, impact duration, and impact location and direction"*.

We agree with the Institute of Medicine as well as Drs. Stapp, McElhaney, Duma and Rowson that single event head impact doses should be collected in vivo, can drive creation of spatial and temporal-based injury criteria, will assist in neurological diagnoses and aide in developing padding designed specifically for on-field impact.

Our goal was to develop a practical head impact instrument implanted in a custom athletic mouthguard and determine if it qualified as a single event dosimeter. Versus Reference Hybrid III 3-2-2-2 accelerometer package, we quantified XYZ component accuracy, precision as well as fit to a linear regression model. We also deployed the Intelligent Mouthguard in American football and boxing to quantify true positive single event frequency content.

A main obstacle we overcame was that the Intelligent Mouthguard gyroscope had insufficient bandwidth, causing amplitude reduction in angular acceleration. This forced us to employ a data-based gyroscope correction and filtering algorithm to correct angular acceleration and velocity before comparing Intelligent Mouthguard to Hybrid III Reference data.

BACKGROUND

Literature

The Head Impact Telemetry System (HITS; Riddell, Elyria, OH) is a well-known American football helmet instrumented with linear accelerometers that transmits single event data to a user on the sideline and stores multiple events in a database. HITS has been used for years to collect and publish large in vivo datasets primarily in American football (Funk et al., 2012; Rowson et al., 2009; Crisco et al., 2010; Duma et al., 2005; Daniel et al., 2012; Rowson and Duma, 2011; Greenwald et al., 2008; Beckwith et al., 2013a; Beckwith et al., 2013b; McAllister et al., 2014; Beckwith et al., 2007). While authors most often report on HITS impact distributions and statistical compilations, single event head impact doses tied to concussion (Mihalik et al., 2010; Guskiewicz et al., 2007b; Guskiewicz and Mihalik, 2010) and cervical fracture (Broglio et al., 2011) have been reported.

Many authors have tested HITS in the laboratory versus Hybrid III Reference headform center of gravity (CG) resultant linear acceleration and angular acceleration. A HITS boxing headgear was tested versus Hybrid III and the authors concluded "…*IBH* (*Instrumented Boxing Headgear) is a valid system for measuring head acceleration and impact location*…" (Beckwith et al., 2007). American football HITS testing versus Hybrid III has demonstrated directional sensitivity – defined as varying accuracy and precision as a function of impact direction – in single events (Jadischke et al., 2013; Siegmund et al., 2014). This is due to inaccurate measurement of tangential acceleration (Rowson et al., 2009) and nonlinear output as function of impact energy and location (Rowson et al., 2011; Siegmund et al., 2014). HITS manufacturers note that one should "*use caution*" when examining single event doses (Beckwith et al., 2012). HITS researchers cite "*greater error*" associated with single event doses (Daniel et al., 2012).

I1 Biometrics (Seattle, WA) makes an instrumented mouthguard (Impact Intelligence System-IIS). X2Biosystems (Seattle, WA) makes an instrumented skin patch (xPatch) and mouthguard (xGuard/DVT3). No peer reviewed publications quantify the performance of the I1 Biometrics' IIS or X2Biosystems' xPatch. Published xGuard/DVT3

tests with a unique impactor and headform found directional sensitivity and resonance (Camarillo et al., 2013). Linear impactor xGuard/DVT3 testing with Hybrid III confirmed directionally sensitive nonlinear acceleration output in single head impact events (Siegmund et al., 2014).

Intelligent Mouthguard

The Intelligent Mouthguard **(Figure 1)** has a 1-Megabit Serial Peripheral Interface Memory Module (EEPROM 25AA1024, Microchip Technology Inc., Chandler, AZ), a microcontroller (dsPIC33FJ128GP804, Microchip Technology Inc., Chandler, AZ), a three-axis angular rate sensor (L3G4200D, ST Microelectronics, Paris, France), and three single axis linear accelerometers (ADXL001-250, Analog Devices Inc., Norwood, MA). We call this the "3a3ω" sensing package.

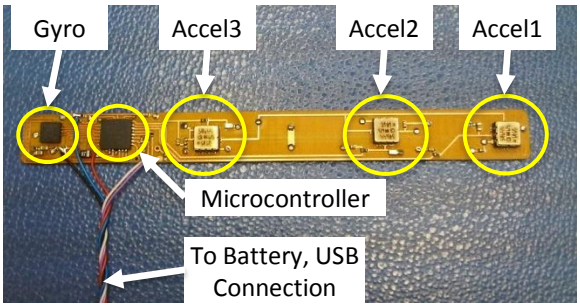

Figure 1. Intelligent Mouthguard 3a3ω sensing package. The gyroscope has on-chip low-pass filtering that attenuates angular acceleration as a function of impact duration. We did Benchtop tests to develop an angular acceleration correction algorithm. We applied this algorithm to Benchtop test data and in vitro XYZ component data.

The flexible printed circuit board is 10mm x 100mm (PCB Fab Express, Sunnyvale, CA) and connected to an external lithium polymer battery (3.7V, 130mAh), on/off switch and mini-USB data offload connector. The Intelligent Mouthguard is capable of sampling up to 4kHz, impact trigger >2g, single event duration up to 125ms and event storage of 200+ events. Each event is time-stamped. Trigger threshold, pre-trigger time, event duration and sample rate are all adjustable. Intelligent Mouthguard sensors have known locations and orientations when laid flat, but have arbitrary locations and orientations when inserted into the mouthguard. In the Methods, we quantify Intelligent Mouthguard sensor location and sensitive axis orientation. Intelligent Mouthguard calculates XYZ linear acceleration temporal traces at any point of interest on the headform; we choose headform CG in this study. Intelligent Mouthguard also calculates XYZ angular acceleration and angular velocity in the headform Reference frame.

Rigid Body Analysis

The Intelligent Mouthguard is used to calculate acceleration of an arbitrary point P in the head, assuming the head is a rigid body. This is determined through the well-known equation,

$$a_p = a_0 + \omega \times r_p + \omega \times (\omega \times r_p) \quad \textbf{(1)}$$

where r_p is a vector of constant length from point O to point P, a_0 is linear acceleration of a point O on the body, angular velocity is ω, and angular acceleration is ω. For a typical in vitro collision, acceleration increases from zero to peak in 5 to 10 milliseconds – defined as Region 1 in our study, see **Figure 2**. The centripetal acceleration term $\omega \times (\omega \times r_p)$ is negligible compared to the tangential acceleration term $\omega \times r_p$ in Region 1. Therefore, accurate determination of arbitrary point acceleration in Region 1 is dependent on the accurate evaluation of translational and tangential accelerations.

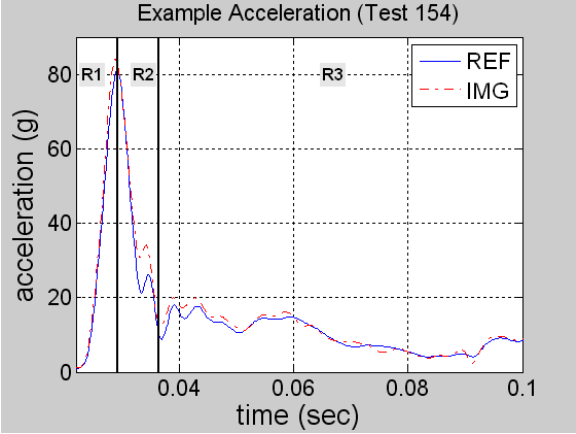

Figure 2. Example Reference and Intelligent Mouthguard temporal response in Region 1 (R1), Region 2 (R2) and Region 3 (R3). We focus on quantifying Intelligent Mouthguard linear regression fit compared to Reference at the time of peak (R1-R2 junction). Up to time of peak, centripetal acceleration is negligible. We also quantify temporal accuracy and precision in R1, R2 and R3. *NOTE: for simplicity, this plot shows resultant CG linear acceleration. All of our calculations are done on XYZ component values at time of peak or XYZ component temporal traces.*

METHODS

We conducted experiments in three phases: (1) Benchtop Component Level Drop Tests, (2) In Vitro System Level Comparison to Reference Linear Impactor Tests and (3) In Vivo Tests (Boxing, American football).

(1) Benchtop Tests

1a. Linear Drop Tests. Our purpose was to compare performance of the Intelligent Mouthguard single axis accelerometers under single axis excitation versus a Reference accelerometer. We conducted tests under similar frequency content and amplitude to what could be expected in sports collisions.

We built a frame out of extruded aluminum to hold a vertical drop rail and a custom carriage with nylon bearings (80/20 Inc., Columbia City, IN). Attached to the carriage was a custom machined fixture to hold the Intelligent Mouthguard printed circuit board. The frame and carriage were mounted to a vibration isolation table **(Figure 3).**

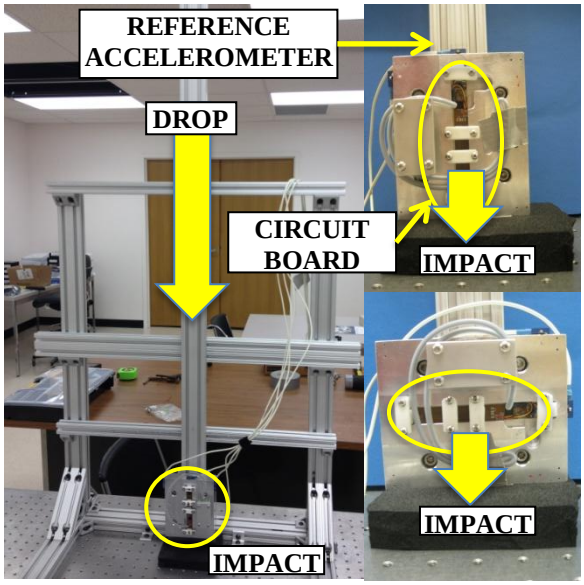

Figure 3. Benchtop linear drop test fixture (left). The Intelligent Mouthguard printed circuit board (circled) is attached in the longitudinal (top right) or lateral (bottom right) direction and dropped from a range of heights (0.076m to 1.067m) onto soft foam and rubber pads.

We instrumented the carriage with Reference linear accelerometers (Model 64B-500, Measurement Specialties, Aliso Viejo, CA) and an angular rate sensor (Model ARS-12k, Diversified Technical Systems, Seal Beach, CA) to measure rotation in-plane. The Reference ARS did not require any correction. We collected Reference data at 10kHz by a National Instruments data acquisition system running Labview software (National Instruments, Austin, TX) and Intelligent Mouthguard data at 4kHz. We used energy absorbing pads; 0.025m thick Durometer 40 foam ("Extra Soft", Part #85175K27, McMaster-Carr, Cleveland, OH) and 0.025m thick neoprene rubber pad ("Medium Hard", Part #9013K87, McMaster-Carr, Cleveland, OH). We conducted 92 linear drop tests (**Table 1**).

Table 1. Benchtop linear drop tests

Test	Drop height (m)	impacts per height
Soft Foam	0.076, 0.178, 0.356, 0.533, 0.711, 0.889, 1.067	6
Rubber Pad	0.127, 0.254, 0.381, 0.508, 0.635	10

In each test Intelligent Mouthguard linear acceleration was compared to Reference using Matlab (Version 2007b, Mathworks, Natick, MA).

1b. Dynamic Rotation Tests. Our purpose was to characterize performance of the Intelligent Mouthguard tri-axial gyroscope versus Reference angular rate sensor (ARS), axis by axis, under single axis excitation. We excited single axes under amplitude and frequency content similar to what could be expected in sports collisions.

The Intelligent Mouthguard printed circuit board was initially motionless on a turntable (Part #9443T2, McMaster-Carr, Cleveland, OH) and we dropped a mass from varying heights to strike the turntable. We used padding (10mm thickness, Airex AG, Sins, Switzerland) attached to the turntable to control contact duration (**Figure 4**).

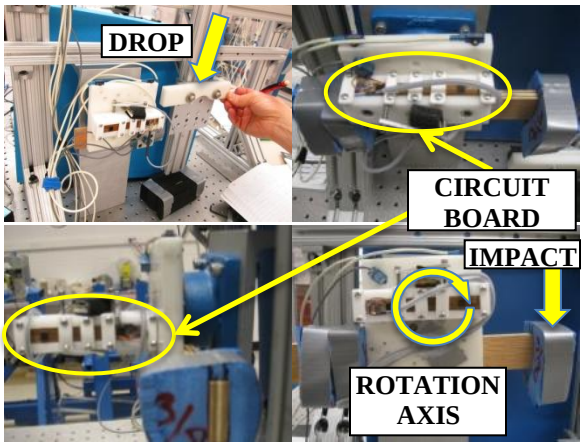

Figure 4. Benchtop dynamic rotation fixture (top left). The Intelligent Mouthguard printed circuit board is attached to the turntable with each gyroscope axis aligned with the rotation axis (top right-Y, bottom left-Z, bottom right-X). The falling mass strikes the turntable arm, inducing rotation. Heights ranged from 0.051m to 0.56m.

Two (2) Reference linear accelerometers (Model 64B-500, Measurement Specialties, Aliso Viejo, CA) were mounted to the rotating fixture on one side and an angular velocity sensor (Model ARS-12k, Diversified Technical Systems, Seal Beach, CA) was mounted parallel to the axis of rotation. Reference data were collected at 10kHz and Intelligent

Mouthguard data at 4kHz. We conducted 42 dynamic rotation tests (**Table 2**).

Table 2. Benchtop dynamic rotation tests

Test	Drop height (m)	impacts per height
10mm Airex	0.051, 0.076, 0.152, 0.254, 0.356, 0.457, 0.559	6

1c. Inadequate Gyroscope Bandwidth and Correction. The gyroscope had a built-in low pass filter – manufacturer specified corner frequency 110 Hz – that caused angular acceleration underestimation. Underestimation worsened with decreasing impact duration. Because of this underestimation, we developed an algorithm to calculate gyroscope correction factors for frequency up to 370Hz. We determined frequency-specific gyroscope correction factors from harmonic simulation and empirical fitting to angular jerk, angular acceleration and angular velocity. Briefly, we determined the correction by simulating test data with 2 harmonics using the MATLAB sin2 function and then applied the algorithm to Benchtop dynamic rotation datasets. In vitro we used Reference acceleration to determine true harmonic content of each signal with the assumption that linear and angular acceleration harmonic contents were comparable. Each of the first two harmonics had their own frequency which were often integer multiples but not always. Each frequency had its own gyroscope amplitude correction at time of Reference peak. We determined the total gyroscope correction factor by superposition of the first two corrected harmonics. If the second harmonic had negligible contribution – less than 5% of Reference amplitude – we ignored this harmonic. We did not modify phase of either harmonic. But more complex data sets, such as resultant linear or angular acceleration having double peaks, could also be modeled in this manner as a linear combination of single data sets with a time delay. This would be possible by modifying harmonic phase(s). The total gyroscope correction we applied was a practical approximation to provide an algorithm-based acceleration peak matching routine. We did not optimize temporal angular acceleration matching in this method. This meant angular velocity mismatch could occur as result of correction; mismatch worsens with increasing harmonic frequency. See **APPENDIX A1** for further details.

(2) In Vitro Linear Impacts

Our purpose was to characterize Intelligent Mouthguard system level performance by comparison against gold standard Reference 3-2-2-2 accelerometer package in a modified Hybrid III headform within given range of acceleration amplitudes and impact durations.

We pressure laminated (Druformat Scan Pressure Machine, DENSTPLY International, York, PA) the Intelligent Mouthguard circuit board (**Figure 5**) onto the headform dentition. We used two, 2mm layers of clear mouthguard polymer (PolyShok™, Sportsguard Laboratories, Kent, OH). The headform dentition was developed for impact testing with Hybrid III (Wonnacott and Withnall, 2010).

Figure 5. In vitro Intelligent Mouthguard fabrication. Printed circuit board placed in machine (top left), Polyshok™ is pre-heated (top right), pressure applied to material, forcing it around board, dentition and dentition embrasure spaces (bottom left). Intelligent Mouthguard ready for testing (bottom right).

We performed 3-2-2-2 Reference calculations (Padgaonkar et al., 1975) in tandem with Reference angular velocity measurement; e.g. a "9a3ω" Reference package (Model 64B-500, Measurement Specialties, Aliso Viejo, CA; Model ARS-12k, Diversified Technical Systems, Seal Beach, CA). In some in vitro American football tests, direct angular velocity measurements were used in the nine accelerometer quadratic terms in place of a faulty satellite accelerometer; see (Kang et al., 2011). A six-axis force-torque transducer was mounted between the head and neck (J1716, Humanetics Innovative Solutions, Detroit, MI) and between the neck and fixed platform (Omega IP65, ATI Industrial Automation, Inc., Apex, NC). The data acquisition system captured Reference data at 10kHz. Signal conditioning and sensor requirements adhered to SAE J211 (Society of Automotive Engineers, 2003). Sign convention adhered to SAE J1733 (Society of Automotive Engineers, 1994). The ram triggered data collection by closing an optical switch positioned to coincide with first contact.

In vitro American football tests used a Varsity Size Large Riddell Revolution Speed IQ HITS Helmet (m=1.87kg) with S2BD-LW-V facemask, Head Impact Telemetry System (HITS, Riddell Inc., Elyria, OH) and a Reebok Checklight skull cap (size large, Reebok International, Canton, MA). In vitro boxing tests used competition boxing headgear (size large, Ringside, Lenexa, KS). The test matrix is shown in **APPENDIX A2.** We co-registered Intelligent Mouthguard sensor position and orientation to the Hybrid III 3-2-2-2 Reference headform using a laser scanner (3D Scanner HD, Next Engine, Inc., Santa Monica, CA). See **APPENDIX A3**. A linear impactor (**Figure 6**, (National Operating Committee on Standards for Athletic Equipment (NOCSAE), 2006) used compressed air to propel at 15kg ram into a stationary Hybrid III 50th percentile head (Humanetics Innovative Solutions, Detroit, MI) at velocities up to 8.5m/s. We attached a 0.025m thick foam pad to the impactor ("Firm", Part #85175K87, McMaster-Carr, Cleveland, OH). We adjusted the target in XYZ with 0.005m resolution and about the Z-axis in 22.5° increments.

Figure 6. Example setups for American football (left) and Boxing (right) Impacts. Intelligent Mouthguard is mounted on the dentition and circled in each image. The linear impactor had a 15kg ram with padded tip that was propelled pneumatically in the horizontal plane into the padded headform. We mounted gold standard 3-2-2-2 Reference accelerometer package inside the headform. A data acquisition system stored Reference data after triggering by light trap at impact; Intelligent Mouthguard data downloaded separately to laptop after each true positive impact.

Friction between the mouthguard and smooth aluminum dentition provided sensor-skull coupling force. We did not physically (finger pressure), visually (high-speed film) or temporally (comparing mouthguard and Reference data) observe significant mouthguard-dentition de-coupling, displacement or transient deformation in any test, including bare head coupling tests up to 286g. Therefore, we omitted clamping forces in vitro because high speed film, pre- and post-test checks and calculation of Intelligent Mouthguard acceleration from Reference confirmed minimal displacement during tests (see **Figure 7**).

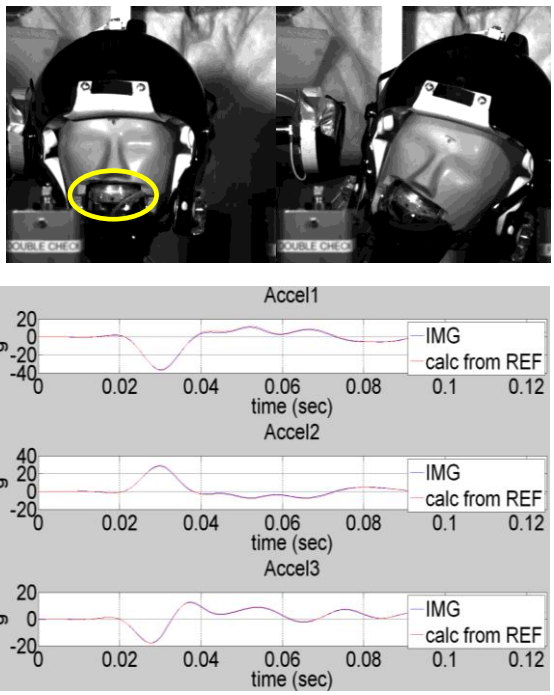

Figure 7. (Top) Coupling is crucial to making accurate headform CG linear acceleration calculations. During tests the Intelligent Mouthguard (circled) remains rigidly coupled to the smooth aluminum dentition. Helmets dynamically de-couple during tests. Post-impact, Intelligent Mouthguard remains firmly coupled in tests up to 286g peak resultant CG linear acceleration. (Bottom) Temporal matching of Intelligent Mouthguard Accel1, Accel2 and Accel3 (IMG - in blue) versus Reference data (calc from REF - in red, dashed) confirms that if de-coupling occurred during testing, it was not enough to create significant temporal mismatch between Intelligent Mouthguard and Reference; the curves are nearly indistinguishable from one another. Test #163 shown in American football 0° Front High Shell, 6.3m/s. This is a typical plot for our in vitro test comparison of Accel1, Accel2 and Accel3 versus Reference.

We used the same data-based gyroscope correction algorithm described in Benchtop Tests and **APPENDIX A1** to correct in vitro temporal angular acceleration and velocity in each X-, Y- and Z-axis. After correcting Intelligent Mouthguard angular acceleration and velocity, we used a Data Translation Algorithm (DTA – see **APPENDIX A4**) to calculate temporal headform CG linear acceleration in each axis.

We also calculated spatial parameters – impact direction and location – at time of peak Reference CG acceleration as detailed in **APPENDIX A5**. Impact Azimuth and Elevation are well understood.

Figure 8. In Vivo Procedure. (left) Build and fit Intelligent Mouthguard. (middle) Boxing and data collection. (right) American football data collection.

Euler Angles define the vector from headform CG to point of impact on the surface of headform. Euler Angles are different than direction cosines of the resultant linear acceleration vector. Any impact line of action can be calculated using Euler Angles, including those impacts where line of action passes through the headform CG. This method allowed us to calculate impact location and direction acting on the headform surface and compare with Reference.

For XYZ component linear regression calculations taken at time of peak, we desired slope and R^2 near 1.00 with y-offset near zero. We also calculated accuracy and precision at the time of peak for XYZ component linear CG and angular acceleration. Finally, we calculated average temporal accuracy and precision in Region 1, Region 2 and Region 3 – see **Figure 2** for further information – for XYZ component linear CG and angular acceleration. To avoid skewing accuracy and precision calculations, we only considered primary impact axes with peak linear acceleration greater than 15g (e.g. our in vivo trigger threshold). Time of peak and temporal calculations provided in **APPENDIX A6**.

(3) In Vivo Impacts

We studied two sets of athletes (Cleveland Clinic IRB13-899): two (2) collegiate American football players and four (4) amateur boxers **(**

Table 3**)**.

Table 3. Human subjects for in vivo impacts. All subjects were male.

Sport	Subject	Age	Ht (m)	Wt (kg)
Boxing	Box995	15	1.68	52
	Box996	17	1.78	75
	Box997	16	1.75	67
	Box999	18	1.78	63
American football	Fball001	19	1.85	105
	Fball002	21	1.93	120

We made a custom Intelligent Mouthguard for each athlete's dentition. During pressure forming the mouthguard material followed each athlete's teeth and embrasure space contours. This ensured coupling to overhanging geometrical irregularities; custom forming is preferable to boil-and-bite forming because boil-and-bite forming only couples firmly to the bite surface. Our dentist ensured each Intelligent Mouthguard fit was tight and comfortable. We did not quantify the removal force necessary to break the mouthguard-dentition geometrical coupling force. But this force in vivo was significant, typically requiring between 4 and 8 fingers to break the mouthguard free from the dentition. The data communication cable exited the mouth and attached to the player's facemask (American football) or headgear (boxing). American football players participated in three, fifteen to thirty minute practice sessions and boxers participated in five, three-minute rounds of sparring. A camera followed each athlete, recording at 60fps. We offloaded data at regular

intervals during practice (American football, ~15-30 minutes) or between each round (boxing, every 3 minutes). We set the trigger threshold to 15g. We collected ten (10) true positive head impact events (**Figure 8**). De-coupling was only observed in between rounds (boxing, when the study team forcibly removed the mouthguard) or during stoppages of play (American football, when the player was not participating).

RESULTS

Benchtop Tests

Linear Drop Tests. An example of linear drop test for Intelligent Mouthguard accelerometer compared with Reference accelerometer data is shown in **Figure 9**. The scatterplot results from all linear drop tests are shown in **Figure 10**.

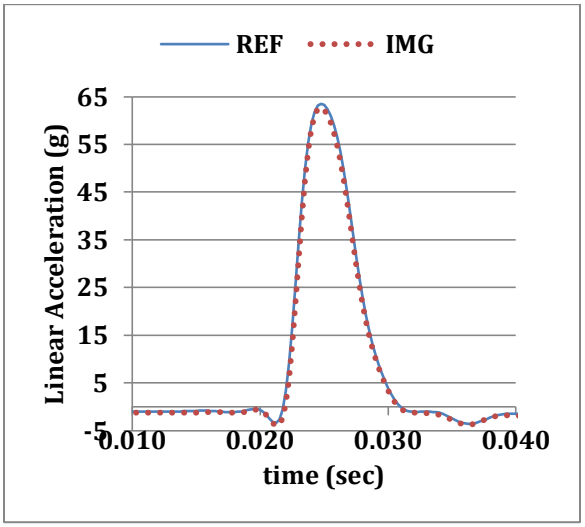

Figure 9. Example linear drop test accelerometer temporal traces; Reference (REF) and Intelligent Mouthguard (IMG). Test #100, drop height =10", rubber pad, peak REF = 63.5g, IMG = 62.8g.

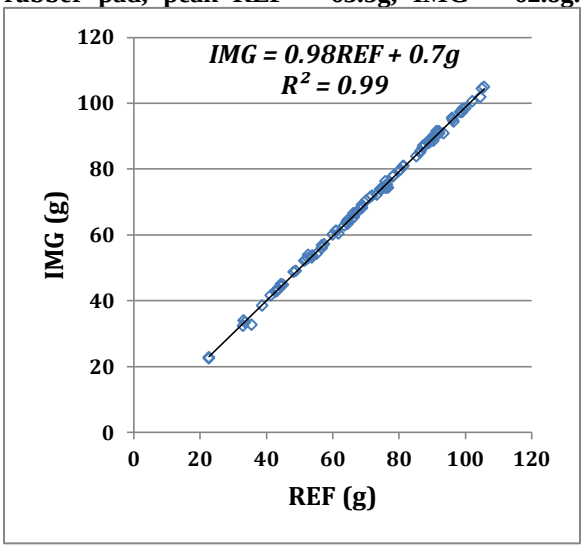

Figure 10. Peak linear acceleration scatterplot for n=92 linear drop tests. We calculated Intelligent Mouthguard accelerometer uncertainty at 3.8% +/-2.0% cross-axis sensitivity (Aksu, 2013).

Dynamic Rotation Tests. An example of a dynamic rotation test showing Reference angular acceleration, Intelligent Mouthguard uncorrected and corrected angular acceleration is shown in **Figure 11**. The calculated frequency response used in correction is shown in **Figure 12**. The peak uncorrected and corrected angular acceleration values for n=42 tests is shown in **Figure 13**.

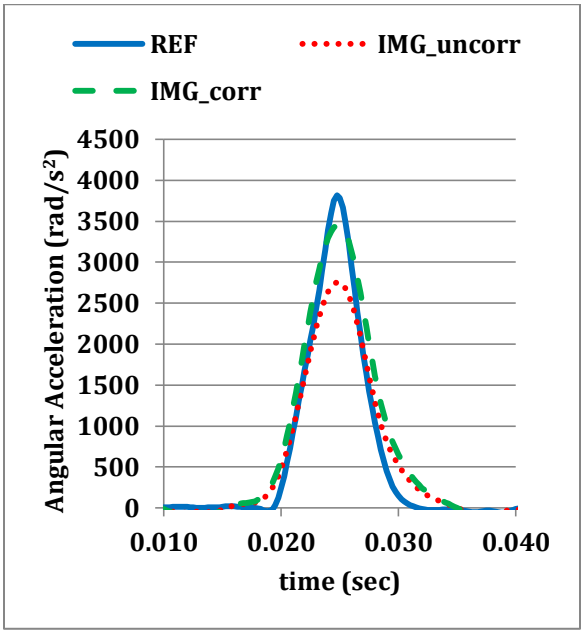

Figure 11. Dynamic rotation temporal example. Test #34, drop height = 0.076m, REF = 3800rad/s^2, IMG_uncorr = 2800rad/s^2, IMG_corr = 3500rad/s^2. First harmonic = 93Hz. Using our harmonic-fitting algorithm, total angular acceleration amplitude correction factor = 1.29.

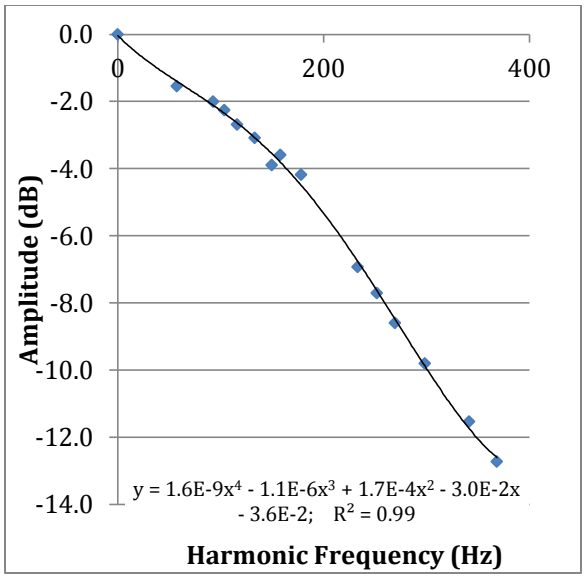

Figure 12. Calculated frequency response and fourth-order fit for Intelligent Mouthguard gyroscope attenuation. We used this frequency response to correct for gyroscope-induced angular acceleration amplitude loss in the first two harmonics.

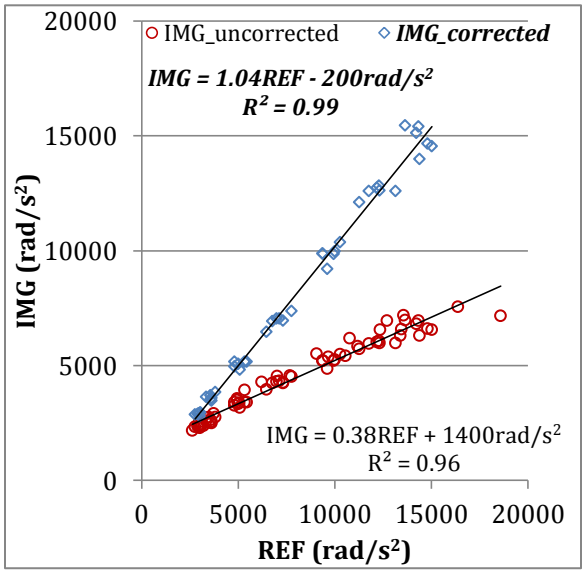

Figure 13. Angular acceleration uncorrected and corrected peak in n=42 dynamic rotation tests. This figure shows the effect of gyroscope peak amplitude loss and corrected peak accuracy after we applied our harmonics-based algorithm. We calculated Intelligent Mouthguard gyroscope output data uncertainty to be 3.3% (Aksu, 2013).

In Vitro Linear Impact Tests

The Intelligent Mouthguard triggered during every in vitro impact, recording a true positive event each time. As opposed to presenting myriad temporal plots, we show an example (**Figures 14 and 15**) of Reference (REF) and Intelligent Mouthguard (IMG) component data for a test with sub-optimal temporal matching to illustrate difference between calculated Intelligent Mouthguard and Reference measured time traces. We summarize in vitro data at the time of peak CG acceleration and temporally in Region 1 (R1), Region 2 (R2) and Region 3 (R3). See **Figure 2** for more information on how we define these Regions.

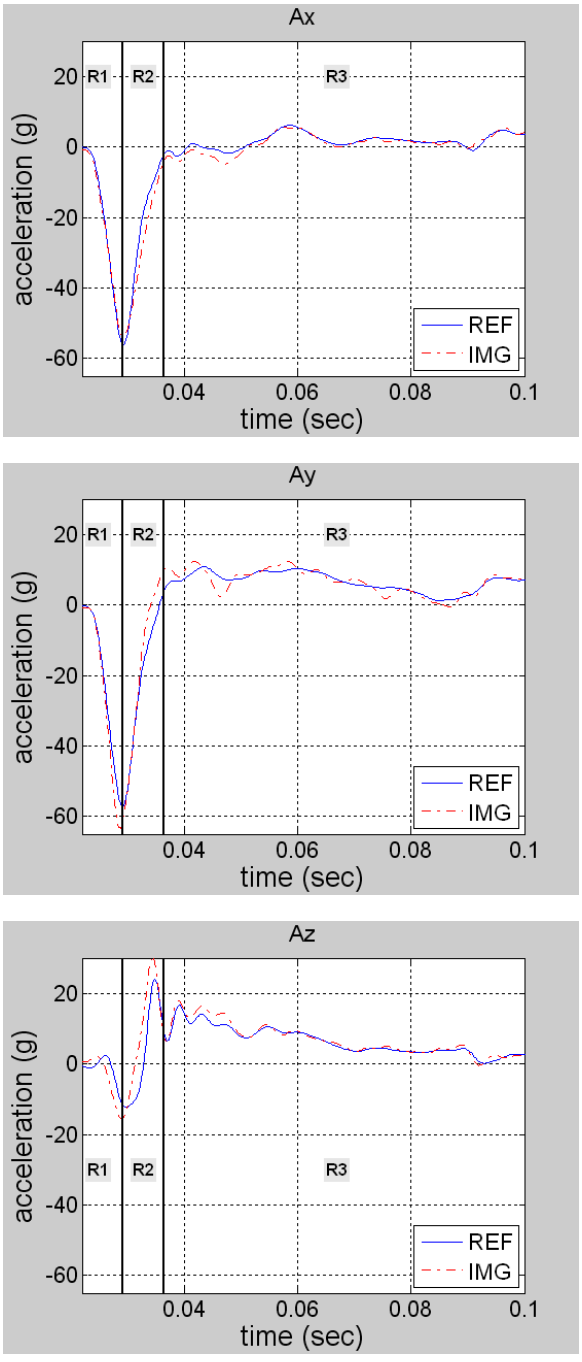

Figure 14. Example headform CG linear acceleration component temporal matching (American football test #151, 7.06m/s, Right Front

(+45°), high. Vertical solid line between R1 and R2 was where we reported peak values. We calculated temporal matching imprecision in R1, R2 and R3.

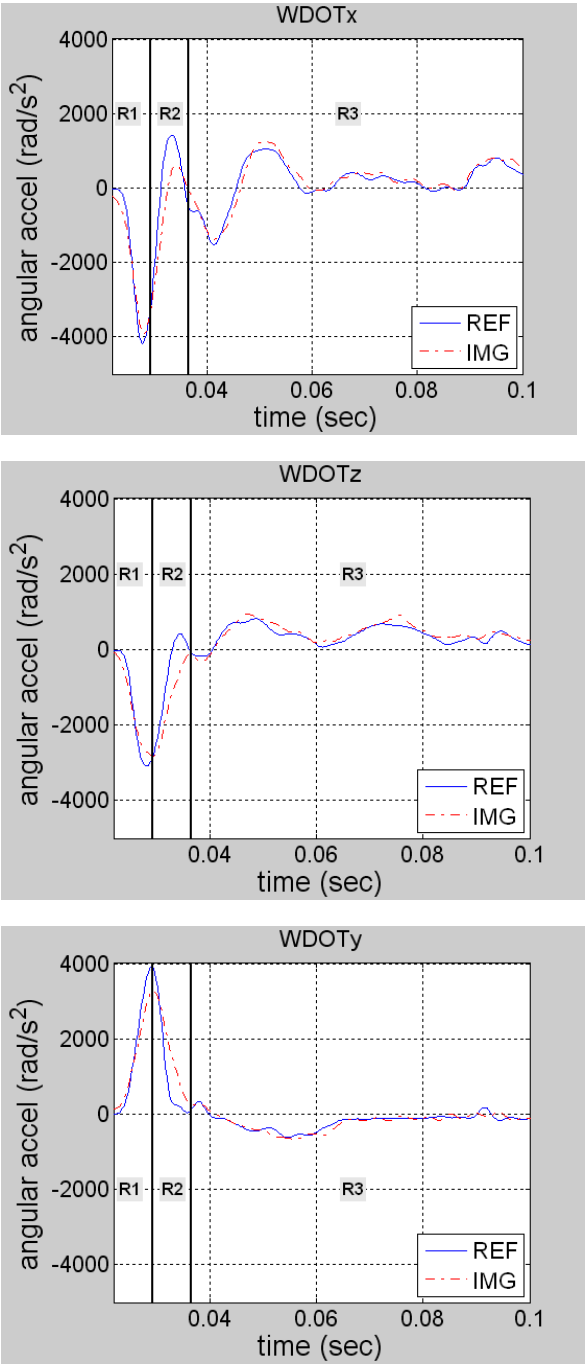

Figure 15. Sample angular acceleration components for test #151. Again, we reported peak values at the R1-R2 junction and we calculated temporal matching imprecision in R1, R2 and R3.

After we quantified XYZ component temporal traces for Intelligent Mouthguard in each test, we calculated average temporal inaccuracy (δ) and precision (σ) for CG linear acceleration and angular acceleration in Region 1, Region 2 and Region 3 as a function of first harmonic frequency (**Table 4**).

Table 4. Intelligent Mouthguard American football (178 tests) and Boxing (68 tests) average temporal accuracy (δ) and precision (σ) as function of first harmonic frequency bin in Region 1, Region 2 and Region 3 for CG linear acceleration and headform angular acceleration. Impact pulse time duration was characterized by the first harmonic frequency (f1). A shorter time duration impulse had a higher f1. A positive value of temporal accuracy meant the average Intelligent Mouthguard temporal trace in a given region was less than Reference. Precision values were quantified at +/-1-σ. Only XYZ components with primary direction of impact acceleration >15g were used.

CG Linear Acceleration temporal accuracy and precision						
American football						
	Region 1 (g)		Region 2 (g)		Region 3 (g)	
f1 (Hz)	δ	σ	δ	σ	δ	σ
<50	0.4	1.3	0.9	1.1	-0.1	0.7
50-70	0.7	1.5	0.8	1.8	-0.1	1.0
71-100	0.9	2.3	1.3	3.3	-0.2	1.3
Boxing						
f1 (Hz)	Region 1 (g)		Region 2 (g)		Region 3 (g)	
	δ	σ	δ	σ	δ	σ
<50	0.1	0.7	1.0	1.0	-0.1	0.8
50-70	0.9	1.7	1.0	2.2	-0.3	0.9
71-100	1.1	2.0	1.4	4.0	-0.8	1.1
Angular Acceleration temporal accuracy and precision						
American football						
	Region 1 (rad/s^2)		Region 2 (rad/s^2)		Region 3 (rad/s^2)	
f1 (Hz)	δ	σ	δ	σ	δ	σ
<50	0	200	20	110	-10	80
50-70	10	200	110	230	-40	100
71-100	10	230	300	390	-90	130
Boxing						
f1 (Hz)	Region 1 (rad/s^2)		Region 2 (rad/s^2)		Region 3 (rad/s^2)	
	δ	σ	δ	σ	δ	σ
<50	20	60	90	90	-50	90

50-70	60	130	280	250	-140	100
71-100	50	180	200	440	-120	90

Figure 16 shows the Intelligent Mouthguard (IMG) and Reference (REF) headform CG linear acceleration XYZ component values taken at the time of peak in American football and Boxing. **Figure 17** shows the angular acceleration scatterplot for XYZ component values reported at time of peak headform CG linear acceleration. **Figure 18** shows the angular velocity scatterplot for XYZ component values taken at the time of peak headform CG linear acceleration.

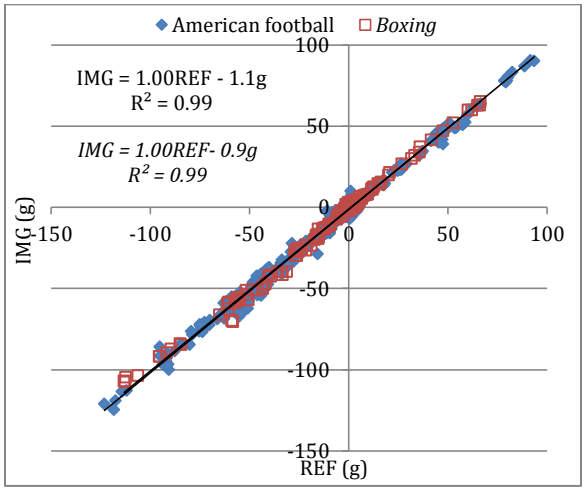

Figure 16. In vitro American football (n=178 tests, 534 XYZ component values at time of peak) and Boxing (n=68 tests, 204 XYZ component values at time of peak) headform CG linear acceleration versus Reference. *Boxing linear regression results italicized.*

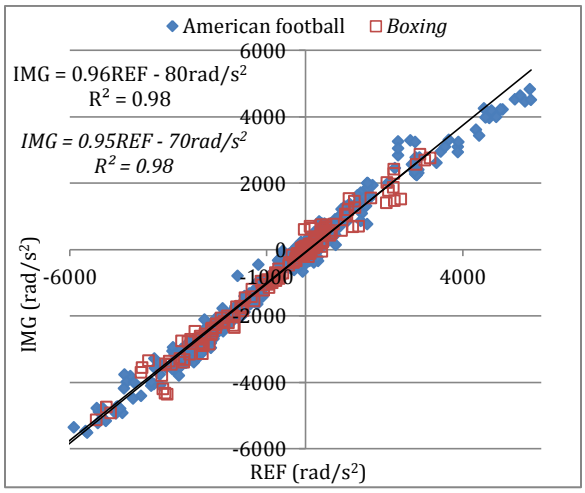

Figure 17. In vitro American football (n=178 tests, 534 XYZ component values at time of peak) and Boxing (n=68 tests, 204 XYZ component values at time of peak) headform XYZ component angular acceleration versus Reference at time of peak linear CG acceleration. *Boxing linear regression results italicized.*

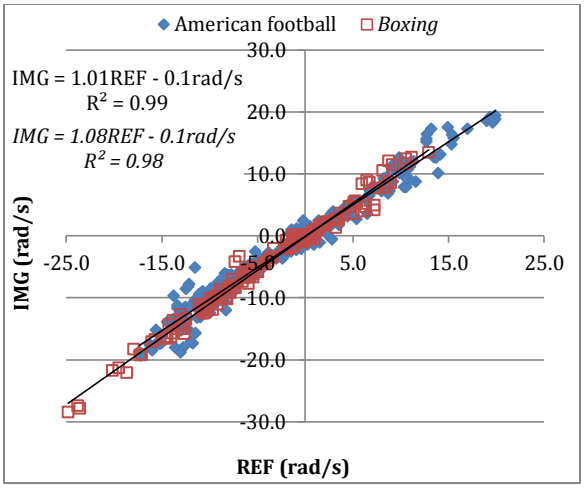

Figure 18. In vitro American football (n=178 tests, 534 XYZ component values at time of peak) and Boxing (n=68 tests, 204 XYZ component values at time of peak) headform component XYZ angular velocity versus Reference at time of peak linear CG acceleration. Angular velocity at time of peak linear CG acceleration is always lower than peak angular velocity. *Boxing italicized.*

We also calculated accuracy and precision at the time of peak in American football and Boxing as a function of first harmonic frequency (**Table 5**).

Table 5. Intelligent Mouthguard accuracy (δ_{pk}) and precision (σ_{pk}) at time of peak in American football (n=178 tests) and Boxing (n=68 tests) as function of first harmonic frequency. A positive value of accuracy meant the average Intelligent Mouthguard value at time of peak was less than Reference. Precision values at time of peak were quantified at +/-1-σ. Only XYZ components with primary direction acceleration >15g included.

f1 (Hz)	Linear CG Acceleration time of peak accuracy and precision			
	American football (g)		Boxing (g)	
	δ_{pk}	σ_{pk}	δ_{pk}	σ_{pk}
<50	2.0	1.7	1.1	1.6
50-70	1.9	3.3	2.8	3.7
71-100	2.0	3.6	0.9	3.9
f1 (Hz)	Angular Acceleration time of peak accuracy and precision			
	American football (rad/s^2)		Boxing (rad/s^2)	
	δ_{pk}	σ_{pk}	δ_{pk}	σ_{pk}
<50	-170	360	70	130

50-70	250	260	120	360
71-100	110	380	-40	390

We quantified Intelligent Mouthguard spatial matching versus the linear regression model of Reference by calculating impact Azimuth, Elevation and Euler Angles using least-squares regression for values taken at time of peak headform CG linear acceleration (**Figures 19, 20 and 21**).

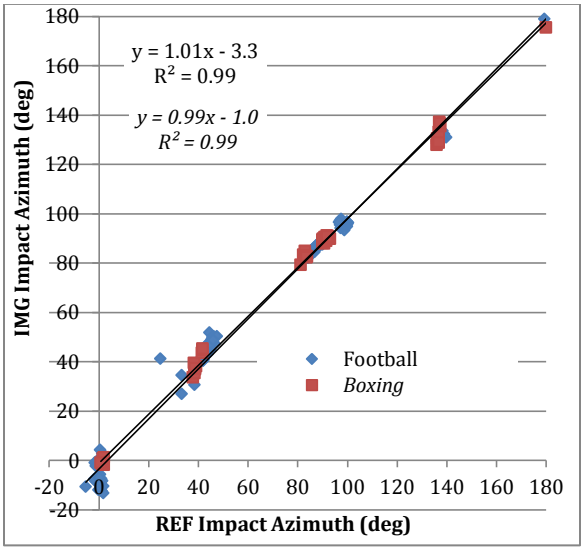

Figure 19. In vitro American football (n=178 tests) and Boxing (n=68 tests) impact azimuth on headform surface for Intelligent Mouthguard and Reference. Azimuth is defined about the headform Z-axis; 0° in front and 180° in rear. Headform surface geometry and moments of inertia the same for Reference and Intelligent Mouthguard calculations. *Boxing linear regression results italicized.*

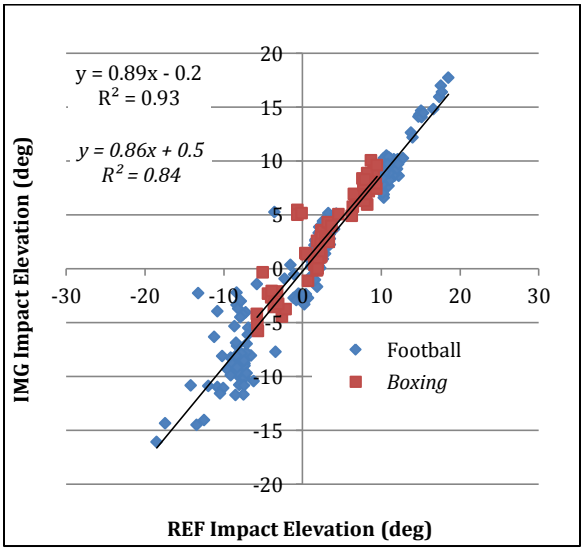

Figure 20. In vitro American football (n=178 tests) and Boxing (n=68 tests) impact elevation on headform surface. Elevation is angle above/below the headform XY-plane; +Elevation points toward the crown. *Boxing linear regression results italicized.*

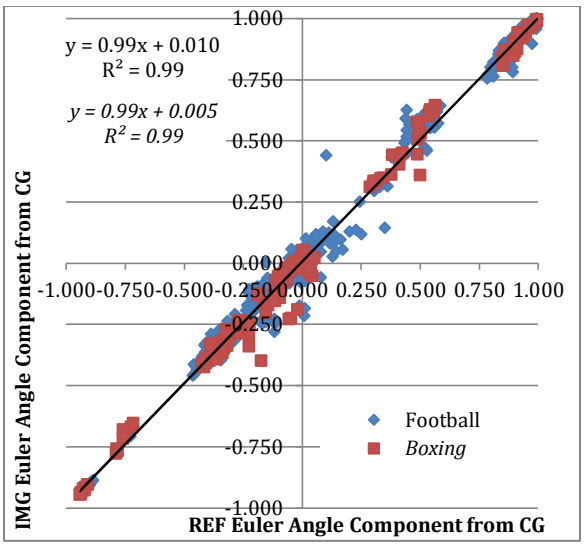

Figure 21. In vitro American football (n=178 tests) and Boxing (n=68 tests) impact Euler Angles. Euler Angles define the vector from headform CG to point of impact on the surface of headform. *Boxing linear regression results italicized.*

We calculated Intelligent Mouthguard precision in impact azimuth (σAz), elevation (σEl) and Euler Angles (σEA) at time of peak CG linear acceleration in American football and Boxing as function of first harmonic frequency (**Table 6**).

Table 6. In vitro Intelligent Mouthguard spatial precision at time of peak for Azimuth (σAz), Elevation (σEl), and Euler Angles (σEA).

American football					
f1 (Hz)	σAz	σEl	σEAx	σEAy	σEAz
<50	3.3°	2.9°	0.041	0.045	0.070
50-70	4.8°	1.9°	0.034	0.069	0.054
71-100	3.2°	2.3°	0.028	0.048	0.039
Boxing					
f1 (Hz)	σAz	σEl	σEAx	σEAy	σEAz
<50	1.8°	1.4°	0.023	0.045	0.054
50-70	2.1°	2.1°	0.027	0.025	0.060
71-100	2.9°	1.1°	0.033	0.049	0.030

In Vivo American football and Boxing Impacts

We calculated first and second harmonic frequencies in Boxing and American football true positive events.

These impacts occurred while the mouthguard was coupled to the athletes' dentition and an obvious impact was observed in video. We synchronized video time and Intelligent Mouthguard time stamps. We determined harmonic frequency in same manner as we outlined for benchtop and in vitro tests. **Table 7** summarizes harmonic findings in n=10 true positive impacts of interest.

Table 7. First and second calculated harmonic frequencies from in vivo boxing and American football Intelligent Mouthguard tests. Any harmonic with amplitude <5% of Reference was assigned f2=0.

Event	f1 (Hz)	f2 (Hz)
Boxing001	61	121
Boxing002	79	161
Boxing005	55	108
Boxing006	36	0
Boxing014	58	154
American football007	48	0
American football008	35	144
American football009	62	121
American football013	39	153
American football015	66	142

We compared our range of first harmonics in American football and Boxing to benchtop and in vitro tests (**Figure 22**).

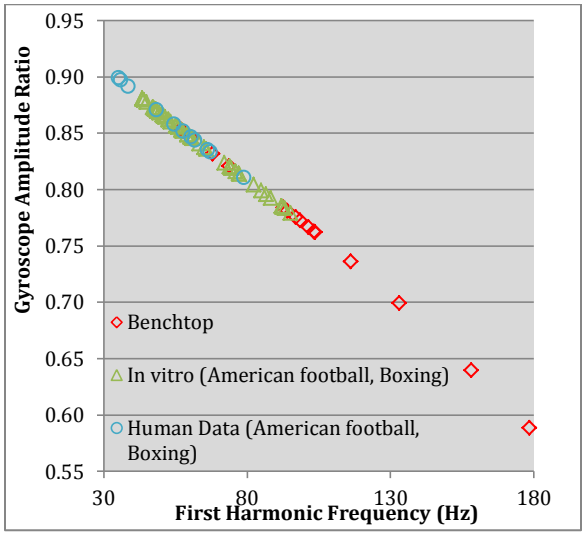

Figure 22. Scatterplot of first harmonic frequency and gyroscope amplitude ratio for in vivo American football and Boxing human data, in vitro American football and Boxing tests and Benchtop tests.

DISCUSSION

In Benchtop drop tests Intelligent Mouthguard accelerometers fit the linear regression model. The gyroscope has a low pass filter that causes data loss when calculating angular acceleration. We overcome this limitation by developing and applying a data-based gyroscope correction algorithm at time of peak. We derive angular acceleration correction factor based on linear acceleration harmonic content.

In dynamic rotation tests, our gyroscope correction data fit the linear model well. The gyroscope angular acceleration correction does not provide perfect temporal matching compared to Reference. This manifests itself in angular velocity mismatch between corrected Intelligent Mouthguard and Reference angular velocity. However, in Region 1 – initial impact loading – the centripetal acceleration magnitude as a function of ω^2 is negligible compared to translational and tangential acceleration. This means that errors in corrected Intelligent Mouthguard angular velocity do not significantly affect the calculation of CG linear acceleration in Region 1.

American football linear CG and angular acceleration temporal average accuracy and precision in Region 1 (δ=0.4 to 0.9g, σ=1.3 to 2.3g; δ=0 to 10rad/s^2, σ=200 to 230rad/s^2), Region 2 (δ=0.9 to 1.3g, σ=1.1 to 3.3g; δ=20 to 300rad/s^2, σ=110 to 390rad/s^2) and Region 3 (δ=-0.1 to -0.2g, σ=0.7 to 1.3g; δ=-10 to -90rad/s^2, σ=80 to 130rad/s^2) increase with increasing frequency content of a signal. Linear CG acceleration, angular acceleration and angular velocity scatterplots at time of peak fit the linear model: IMG = 1.00REF – 1.1g, R^2 = 0.99, IMG = 0.96REF – 80rad/s^2, R^2 = 0.98, IMG = 1.01REF – 0.1rad/s, R^2 = 0.99. Linear CG acceleration precision decreases with increasing harmonic signal content (maximum 3.6g). Linear CG (1.9 to 2.0g) and angular acceleration (-170 to 250rad/s^2) accuracy do not decrease with increasing harmonic signal content. Angular acceleration precision varied from 260 to 370rad/s^2. Impact Azimuth (IMG=1.01REF – 3.3°, R^2=0.99), Elevation (IMG=0.89REF – 0.2°, R^2=0.93) and Euler Angles (IMG=0.99REF – 0.010, R^2=0.99) fit the linear model. Impact Elevation has the worst slope, but the 11% error translates into a modest 2° error at our tested limits. Time of peak precision is 3.2 to 4.8° in Azimuth and 1.9 to 2.9° in Elevation and did not depend upon harmonic signal content.

Boxing linear CG and angular acceleration temporal average accuracy and precision in Region 1 (δ=0.1 to 1.1g, σ=0.7 to 2.0g; δ=20 to 60rad/s^2, σ=60 to 180rad/s^2), Region 2 (δ=1.0 to 1.4g, σ=1.0 to 4.0g; δ=90 to 280rad/s^2, σ=90 to 440rad/s^2) and Region 3 (δ=-0.1 to -0.8g, σ=0.8 to 1.1g; δ=-50 to -140rad/s^2, σ=90 to 100rad/s^2) increase with increasing frequency content of a signal. Linear CG acceleration and angular acceleration scatterplots at time of peak fit the linear model: IMG = 1.00REF – 0.9g, R^2 = 0.99, IMG = 0.95REF – 80rad/s^2, R^2 = 0.98, IMG =

1.08REF – 0.1rad/s, R^2 = 0.98. Linear CG acceleration and angular acceleration precision decreases with increasing harmonic signal content (maximum 3.6g and 390rad/s^2). Linear CG (0.9 to 2.8g) and angular acceleration (-40 to 120rad/s^2) accuracy do not increase with increasing harmonic signal content. Impact Azimuth (IMG=0.99REF – 1.0°, R^2=0.99) and Euler Angles (IMG=0.99REF + 0.005, R^2=0.99) fit the linear model. Impact Elevation (IMG=0.86REF + 0.5°, R^2=0.84) has the lowest accuracy and worst linear fit, but the 14% error translates into acceptable 2° error at our tested limits. Time of peak precision is 1.8 to 2.9° in Azimuth and 1.1 to 2.1° in Elevation.

With increasing frequency of harmonic content of a signal, we find increasing imprecision in calculated CG linear acceleration. Therefore, there is a practical limit to applicability of our 3a3ω hardware platform due to gyroscope bandwidth limitations. We define this limit as less than 100Hz in the first harmonic for American football and Boxing. Within this limit, the angular acceleration temporal precision for any axis in any of our tests in Region 1 is less than 230rad/s^2. Assuming 8cm axial distance from head CG to angular acceleration measurement point in the mouth, this precision equates to 2.9g, comparable to our maximum time of peak (3.9g) and temporal (2.3g) linear CG acceleration precision.

From our American football (n=2 players) and amateur boxing (n=4 boxers) we report on frequency content in ten true positive head impact events. The first harmonic frequency (35Hz to 79Hz) in these events is within our tested benchtop and in vitro ranges. These subjects have harmonic frequency content well below the 828Hz to 1417Hz in vivo skull resonant frequency (Hakansson et al., 1994). We consider the live subjects events and their kinematics as non-concussive because no athlete sustained a diagnosed concussion while wearing Intelligent Mouthguard.

Our results are based on Intelligent Mouthguard comparison to Reference Hybrid III headform to determine whether Intelligent Mouthguard qualifies as a single event dosimeter within our tested ranges and configurations. These ranges are: American football and Boxing, first harmonic frequency less than 100Hz, XYZ component linear acceleration -123g to +92g and XYZ component angular acceleration -5900rad/s^2 to 5700rad/s^2. It is of limited value to compare our findings with published data acquired and analyzed differently, especially for devices not intended for use as single event dosimeters. Also, we cannot objectively compare our results with any other results without knowing harmonic signal content ranges and ensuring tests are done under comparable conditions. Regardless, we briefly report published data on other head impact instruments tested in vitro.

Beckwith et al. tested a 12-accelerometer Head Impact Telemetry System "Instrumented Boxing Headgear" (HITS "IBH") in 56 Hybrid III linear impacts up to 77g and 6400rad/s^2 resultant linear and angular acceleration, respectively (Beckwith et al., 2007). They found temporal bias in resultant was 6g (1-σ imprecision 3g) and 600 rad/s^2 (1-σ imprecision 400rad/s^2), respectively. Harmonic signal content of their tests was unknown. They did not report on temporal or peak component matching. Beckwith et al. (2007) concluded "*The results of this study demonstrate that measurements of head acceleration using this instrumented boxing headgear are well correlated with comparable measures.*"

Rowson et al. tested a twelve-accelerometer Riddell Revolution HITS American football helmet in 114 linear impacts with Reference Hybrid III up to resultant 176g and 14,400 rad/s^2 (Rowson et al., 2011). They reported a power fit between HITS and Hybrid III peak resultant linear (Hybrid III = 0.87*HITS$^{1.06}$) and angular acceleration (Hybrid III = 0.06*HITS$^{1.37}$). Temporal bias in resultant was 12g (1-σ imprecision 8g) and 900 rad/s^2 (1-σ imprecision 700rad/s^2), respectively. Harmonic signal content of their tests was unknown. Rowson et al. did not report on XYZ component temporal or peak matching. Rowson et al. (2011) concluded "*This technology provides the opportunity to collect a large and unbiased dataset*."

Beckwith et al. tested a six-accelerometer Riddell Revolution HITS helmet in 73 Hybrid III linear impacts up to approximately 190g and 12000rad/s^2 resultants (Beckwith et al., 2012). They found directional sensitivity as a function of impact configuration in linear acceleration and angular acceleration peak resultants. They also found Head Injury Criterion (HIC), a temporal matching surrogate, had directional sensitivity. Linear regression, which was forced to have zero y-offset, produced slope ranging from 0.97 to 2.92 in peak resultant linear acceleration, 0.55 to 2.23 in peak resultant angular acceleration and 0.41 to 4.36 in HIC. Harmonic signal content of their tests was unknown. They did not report on XYZ component temporal or peak matching. Beckwith et al. (2012) concluded "*…researchers should use caution when analyzing results from isolated events… distributions of measurements obtained on-the field with the HIT System will be nearly identical to those obtained in the laboratory as long as the laboratory tests reflect field conditions*."

Jadischke et al. confirmed Beckwith et al.'s (2012) findings after adding 28 additional linear impact tests

up to 82g and 5700rad/s^2 peak resultants (Jadischke et al., 2013). They also found HITS did not report data in 25% of additional tests. Jadischke et al. did not report on XYZ component temporal or peak matching. Harmonic signal content of their tests was unknown. Jadischke et al. (2013) concluded "*Head accelerations from HIT are less inaccurate for shell than facemask impacts. However, they are not accurate enough to predict head biomechanics in helmet impacts... facemask impacts appear erroneously high and should not be included in any risk curve computation.*"

Camarillo et al. tested the X2 Biosystems mouthguard using a custom headform and spring-loaded impactor in 128 tests generating resultant peaks up to 152g and 11,500rad/s^2 (Camarillo et al., 2013). Harmonic signal content of their tests was unknown. The X2 Biosystems mouthguard had the same gyroscope model (L3G4200D) as Intelligent Mouthguard. Camarillo et al. quantified directional sensitivity in linear regression of peak resultant linear acceleration (slope 0.92 to 1.21) and angular acceleration (slope 0.77 to 1.44) with y-offset forced to be zero. They noted errors due to sagittal plane resonance and gyroscope amplitude attenuation. We know these errors combine unpredictably and increase single head impact event measurement uncertainty. Camarillo et al. (2013) concluded that "*...it is difficult to ascertain if errors due to high frequency content in a laboratory test are meaningful or irrelevant.*" In our tests, in vivo and in vitro harmonic contents of impact signals are comparable. Therefore, in vivo and in vitro gyroscope correction is necessary, relevant and provides a meaningful reduction in single event uncertainty as a function of harmonic content of single event impact signals.

Siegmund et al. tested the Riddell Revolution Speed HITS and the X2 Biosystems mouthguard using a Hybrid III in 896 tests up to approximately 200g peak resultant CG linear acceleration and 15,000rad/s^2 peak resultant angular acceleration (Siegmund et al., 2014). They reported that HITS and X2 both had directional sensitivity and both had non-linear output as Reference amplitude increased. Omitting crown, oblique and eccentric #1 tests from consideration, power fits deviated from desired slope of 1.00; HITS had power-fit slope range of 0.67 to 2.72 and X2 had power-fit slope range from 0.96 to 1.84. The power-fit exponent also deviated from the desired 1.00; HITS had power-fit exponent ranging from 0.72 to 1.00 and X2 power-fit exponent ranged from 0.84 to 1.04. They did not report on XYZ component peak or temporal matching. Harmonic impact content of signals was unknown. Siegmund et al. (2014) concluded that Riddell Revo Speed HITS and X2 Biosystems mouthguard "*have potential to accurately quantify impact severity…*" and "*…there are major limitations in both systems as tested.*"

The Institute of Medicine recently recommended that "*…research on age- and sex-related biomechanical determinants of injury risk for concussion in youth… are critical for informing the development of rules of play, effective protective equipment and equipment safety standards, impact-monitoring systems, and athletic and military training programs…*" and that "*…none of the risk curves in the literature comprehensively account for parameters such as impact direction…"* (Institute of Medicine and National Research Council, 2014). A single event head impact dosimeter helps to address these challenges. There is no quantitative industry standard that defines whether or not an instrument is a single event head impact dosimeter. Our approach to creating a single event head impact dosimeter is to develop a practical instrument that maximizes accuracy and minimizes single measurement uncertainty within reason.

Based on our results, Intelligent Mouthguard is a single event head impact dosimeter in American football based on component fit to linear regression versus Reference (IMG=1.00REF-1.1g, R^2=0.99; IMG=0.96REF-80rad/s^2, R^2=0.98), time of peak XYZ component maximum imprecision (3.6g, 370rad/s^2), maximum time of peak azimuth and elevation imprecision (4.8° and 2.9°) and maximum average temporal imprecision (3.3g and 390rad/s^2). Average American football XYZ component temporal and time of peak accuracy is approximately 2g or less than Reference for all tests. Intelligent Mouthguard is also a single event head impact dosimeter in Boxing based on component fit to linear regression versus Reference (IMG=1.00REF-0.9g, R^2=0.99; IMG=0.95REF-70rad/s^2, R^2=0.98), time of peak maximum XYZ component imprecision (3.9g, 390rad/s^2), maximum azimuth and elevation imprecision (2.9° and 2.1°) and maximum average temporal imprecision (4.0g and 440rad/s^2). Average boxing XYZ component temporal and time of peak accuracy is approximately 3g or less than Reference for all tests. Intelligent Mouthguard is a single event head impact dosimeter only within our tested amplitudes and harmonic signal content ranges for true positive events.

Limitations

We did not test the Intelligent Mouthguard components or system under every conceivable configuration. If in vitro or in vivo data are acquired in the future that reside outside the boundaries of validated range of harmonic content or sensor-skull coupling we studied, further validation may be needed to quantify data accuracy or such data may need to be rejected. This is especially important for

higher frequency impacts with first harmonic >100Hz. For higher frequency impacts, a wider-bandwidth instrument may be needed to accurately quantify impact kinematics. There is, however, a practical limit to measuring head impact doses in a wider-bandwidth instrument when harmonic content of impact signals approach the in vivo skull resonant frequencies of 828Hz to 1417Hz (Hakansson et al., 1994). Any instrument that relies upon rigid body assumptions may suffer increased measurement uncertainty as the impact kinematics excite frequencies near skull resonant frequencies.

We also did not quantify mouthguard-dentition coupling force. Dentition geometry provides mouthguard coupling friction. All in vitro tests were performed on a smooth aluminum dentition with vertical sides, without lower jaw clamping. We have no data-based evidence of de-coupling in vitro. In vivo, our human subjects lubricate the dentition with saliva. Saliva likely decreases coupling force. But human dentition complexity and embrasure spaces provide geometrical benefits that increase chances of the mouthguard remaining coupled during and after a collision. High quality dental work in manufacturing a custom mouthguard further provides assurance of best possible coupling for a given dentition. The Intelligent Mouthguard used in our boxer testing required two-handed effort by a dentist for de-coupling. We have no data-based evidence of de-coupling in humans.

Practical Considerations and Future Work

Our current results focus on accurately and precisely calculating peak acceleration and time traces for any point on the head during and immediately after impact in vitro. In the future we will expand these calculations to live athletes when single head impact event uncertainties in vivo must also be quantified. As part of this effort, we must quantify Intelligent Mouthguard sensor positions and sensitive axis orientations for each subject with respect to each subject's unique head anthropometry. We will use a valid magnetic resonance imaging method to do so in the future (Ozturk, 2013). This method allows us to reduce uncertainty and report subject-specific head kinematics.

For the chosen 3a3ω hardware platform, the practical limit of gyroscope-based angular acceleration correction is when first harmonic frequency is less than 100Hz. Future work will include improving bandwidth for accurate evaluation of shorter time duration pulses, such as bare head impacts. In the future we will expand Intelligent Mouthguard application to temporal regions where angular velocity gains importance.

Each impact trace is estimated by six constants for amplitude, frequency and phase of the two harmonics. We call this data compression because we have greatly reduced – from hundreds/thousands to a few dozen – the number of data points to estimate each kinematic trace. Data compression will be useful in future work in order to store more single head impact events on-mouthguard and reduce number of data points to transmit wirelessly in real time.

Finally, we know any future practical single event dosimeter requires low power consumption, wireless data transfer, high sensitivity, high specificity and sufficient bandwidth for padded and non-padded head impacts. Future Intelligent Mouthguard versions will incorporate these features.

CONCLUSIONS

Our study conclusions apply only to the situations where the rigid body assumption is valid, sensor-skull coupling is maintained and the ranges of tested parameters and harmonics generated fall within the boundaries of harmonics validated in vitro.

Intelligent Mouthguard spatial and temporal data correlate in a linear model to the Reference Hybrid III within our tested range of pulse durations and impact acceleration profiles in American football and Boxing in vitro tests.

In vivo Intelligent Mouthguard true positive head impacts from American football and amateur boxers have harmonic content within our tested ranges for benchtop and in vitro experiments.

Intelligent Mouthguard qualifies as a single event dosimeter in American football and Boxing within our tested amplitudes and harmonic signal content ranges for true positive events.

ACKNOWLEDGMENTS

This study was supported by Cleveland Clinic Neurological Institute, Cleveland Clinic Center for Spine Health, Cleveland Clinic Stanley Zielony Spinal Surgery Research & Education Fund, Cleveland Clinic Research Program Committee, Cleveland Clinic Innovation Development Fund, National Football League Charities, Orthopaedic Research and Education Fund, Cleveland Traumatic Neuromechanics Consortium, Rawlings Performance Institute at Cleveland Clinic, Sportsguard Laboratories and the George and Grace Crile Traveling Fellowship. From Cleveland Clinic, we thank Farhad Bahrehmand, Barry Kuban, Cristian Pasluosta and Kevin Waters for electrical engineering assistance, Basar Aka, Alper Aksu, Jay Alberts PhD, Andrew Bayzik Erik Beall PhD, Andrew Healy MD,

Erica Heisler, Josh Hirsch, Mark Lowe PhD, Caglar Ozturk, Victor Perhay, Brach Poston PhD and Anno van den Akker, for data collection help, Tara Bonner, Robb Colbrunn PhD, Rob Daniels, Ryan Klatte and Anthony Shawan for engineering support, Gordon Bell MD, Anne Castellano, Jane Kasper, Michelle Marcus, Brian Perse and Susan Rossi for research support. We thank Dave Conger, Neil Harnar and Vikas Prakash PhD from Case Western Reserve University for testing assistance. We thank Zach Brett and Rick Sepi from Sportsguard Laboratories for mouthguard manufacturing assistance. From Ricardo Cavalcanti Brazilian Jiu-Jitsu Gym, we thank Gil Martinez, his amateur boxing team and their parents. From Kent State University, we thank Marc Johnson, Trent Stratton ATC and the coaches. Finally, we thank Dominique Barbier, Jay Esfandyari and Marco Ferraresi from ST Microelectronics for assistance with gyroscope low-pass filtering.

APPENDIX

A1. Harmonic Content

The Intelligent Mouthguard L3G4200D gyroscope has a built-in, low-pass linear phase filter. Under impact conditions involving signals with harmonic content of higher frequencies, this filter causes unacceptable output signal attenuation which increases inaccuracy in calculated temporal and spatial head impact parameters.

The motivation for determining harmonic content of impact signals was to (1) restore original angular velocity and angular acceleration data from the filtered L3G4200D gyroscope angular velocity data for head impact frequencies where signals were attenuated and (2) determine practical limits for applicability of such restoration technique.

Conceptual proof of the need for angular acceleration correction. To evaluate frequency content of a single head impact test data set, we simulated experimental data for Region 1, Region 2 and Region 3 (see **Figure 2** for clarification), using harmonic approximation of time derivative of angular acceleration (see **Figure A1-1**).

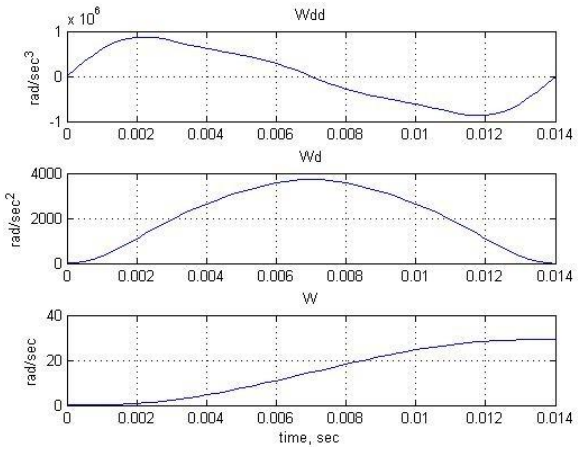

Figure A1-1. Simulated single head impact experimental data: time traces for angular velocity ω (BOTTOM), angular acceleration ω(MIDDLE), time derivative of angular acceleration ω (TOP). T=0.014s.

The time derivative of angular acceleration can be approximated as a sum of harmonics:

$$\omega = \sum_{i}^{N} \omega_i$$

$$\omega_i = a_i * \sin\ \frac{2 \times \pi \times i}{T} \times t + \varphi_i$$

Where i is a harmonic number,
T is a characteristic time period for the signal,
a_i is a harmonic amplitude,
t is a time variable,
φ_i is a harmonic phase at $t=0$.

The total number of harmonics N is determined by how closely the approximation must follow the measured data. For convenience we introduce i_{th} harmonic frequency

$$\Omega_i = \frac{2\pi i}{T}$$

where $\Omega = \frac{2\pi}{T}$ is a fundamental frequency, then

$$\omega_i = \boldsymbol{a_i * \sin\ \Omega_i t + \varphi_i} \qquad \textbf{(A1-1)}$$

The angular acceleration approximation becomes

$$\omega = \sum_{i}^{N} \omega_i$$

with

$$\omega_i = \frac{a_i}{\Omega_i} \times \boldsymbol{\cos\ \varphi_i\ - \cos(\Omega_i t + \varphi_i)} \qquad \textbf{(A1-2)}$$

and the angular velocity harmonic

$$\omega_i = \frac{a_i}{\Omega_i}\cos(\varphi_i) \times t - \frac{a_i}{\Omega_i^2}\sin(\Omega_i t + \varphi_i) - \sin(\varphi_i)$$

$$\omega_i = \frac{a_i}{\Omega_i^2}\mathbf{sin}(\boldsymbol{\varphi_i}) + \frac{a_i}{\Omega_i}\mathbf{cos}(\boldsymbol{\varphi_i}) \times \boldsymbol{t} - \frac{a_i}{\Omega_i^2}[\mathbf{sin}(\boldsymbol{\Omega_i t})\mathbf{cos}(\boldsymbol{\varphi_i}) + \mathbf{cos}(\boldsymbol{\Omega_i t})\mathbf{sin}(\boldsymbol{\varphi_i})] \quad \textbf{(A1-3)}$$

The angular velocity signal is the one which is filtered; the components of this signal are a constant, a linear term and harmonics,

$\frac{a_i}{\Omega_i^2}\sin(\varphi_i)$; $\frac{a_i}{\Omega_i}\cos(\varphi_i) \times t$; $-\frac{a_i}{\Omega_i^2}\cos(\varphi_i)\sin(\Omega_i t)$ $-\frac{a_i}{\Omega_i^2}\sin(\varphi_i)\cos(\Omega_i t)$

The linear term frequency content can be evaluated through its Fourier series.

Linear acceleration has harmonic approximation per equation (**A1-2**). We used linear acceleration to define the signal harmonic content.

Frequency content of such simulated experimental data in our tests exceeded the known corner frequency of the gyroscope low pass filter, especially for the shorter duration impacts (lower T value). Therefore, we had to determine a practical way of implementing a data based correction.

Data Based Gyroscope Correction Method Using Harmonics

We used a method to minimize error in harmonic fitting to angular velocity and angular acceleration. Error minimization depended upon record length of fit, also known as Tfit. We calculated an error function (f_{err}), first harmonic (f1) and second harmonic (f2) as a function of Tfit. Two harmonic components proved to be sufficient for adequate representation of the experimental data. The data based correction factors were determined as follows:

1. Pre-filter Reference with a 6th order low-pass Butterworth filter (1650Hz corner frequency).
2. Numerically differentiate and integrate Reference acceleration to determine jerk and velocity, respectively. Jerk is re-filtered with same filter as in 1.
3. Calculate amplitude (a_1, a_2), frequency (f_1, f_2) and phase (ϕ_1, ϕ_2) for each of first two harmonics (via Matlab 'sin2' fitting algorithm) that best fits jerk, acceleration and velocity. The basis for this fit – and all other fitted data in the study – is Equation (**A1-3**). We quantify record length, Tfit, by the presence of a local minimum on an error function:

$$\boldsymbol{f_{err}} = \sqrt{\mathbf{1} - \boldsymbol{AR_{acc}}^{\,2} + \mathbf{1} - \boldsymbol{AR_{vel}}^{\,2} + \mathbf{1} - \boldsymbol{R_{acc}^2}^{\,2} + \mathbf{1} - \boldsymbol{R_{vel}^2}^{\,2}} \quad \textbf{(A1-4)}$$

Where AR_{acc} is the amplitude ratio of the calculated sum of acceleration harmonics divided by Reference at time of peak acceleration,

AR_{vel} is the amplitude ratio of the calculated sum of velocity harmonics divided by Reference at the time of peak acceleration,

R_{acc} is the r-squared of the temporal fit between Reference and calculated sum of acceleration harmonics for the record duration,

R_{vel} is the r-squared of the temporal fit between Reference and calculated sum of velocity harmonics for the record duration,

4. The f_{err} is plotted versus record length +/- point of peak acceleration (jerk~0) and frequency slope <1Hz/point. **Figure A1-2** shows an example of the harmonics and f_{err} *1000. Each optimum fitted record length is confirmed by plotting harmonic calculated fit versus Reference kinematics for jerk, acceleration and velocity. **Figure A1-3** shows an example of the fits for test #58. The fitted harmonics quantify Reference harmonic frequency and amplitudes fit. These were considered 'true' harmonic values.
5. The gyroscope first (f_1) and second (f_2) harmonic correction are calculated by dividing true harmonic amplitude (**Figure A1-3**) by attenuated gyroscope amplitude ratio (see **Figure 12**) at each harmonic frequency. If any harmonic correction was <0.05, this harmonic is forced to zero (e.g. f_2=0, $corr_2$=0). After calculating the correction factors at each harmonic frequency, the total gyroscope correction is calculated for each test by superposition of the f_1 and f_2 corrections. The total gyroscope correction is then multiplied to the entire angular velocity and angular acceleration XYZ component time series.
6. The cutoff filter frequency is set to the max(f_1,f_2). If f_2=0, cutoff frequency=f_1.
7. After calculating cutoff frequency, the imported Reference data were resampled to 4kHz. REF data are filtered with a 6th order low-pass Butterworth at calculated cutoff frequency.

8. Filter Intelligent Mouthguard data with same 6th order low-pass filter as Reference.
9. Synchronize Reference and Intelligent Mouthguard linear acceleration data at time of peak and report data in point-slope correlation scatterplot.

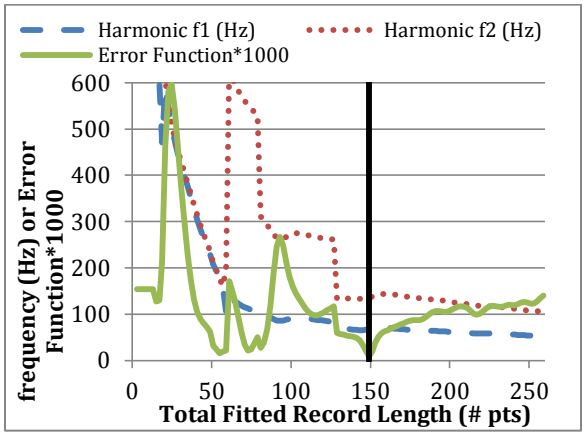

Figure A1-2. Linear Drop Test example of fitted harmonics (f_1, f_2) and error function ($f\ err$ *1000). Test #58, 1.067m drop height, soft foam, optimum fitted record length, T_{fit}, 149 points denoted by vertical solid line.

Practical Considerations

Effectiveness of our reconstruction method to a large degree depends on the appropriate selection of $\boldsymbol{\Omega} = \frac{2\pi}{T}$, where T is the time period when acceleration increases from zero to maximum value and goes back to zero (or angular velocity increases from zero to its maximum value). We made this process algorithmic and data-based by determination of T_{fit} through minimization of error function (eq. **A1-4)**. Another restriction on this method of reconstruction is imposed by a noise level in the measured signals. Recovery of a severely attenuated signal, which has amplitude not much higher than the noise in the measurement, is inaccurate. This imposes a high frequency limit beyond which reconstruction is not possible.

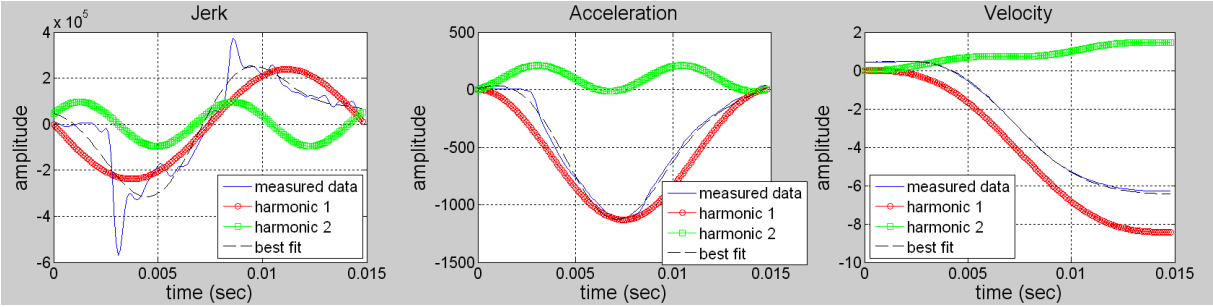

Figure A1-3. Harmonic fitting Step 5 for Linear Drop Test #58. 'Best fit' defined the true harmonic content from Reference (e.g. frequencies and amplitude ratios).

A2. In Vitro Tested Ranges

Test Condition	Headform Configuration (Azimuth)	Velocity Range (m/s)	Total Impacts	Impacts with harmonic1 <100Hz	Test Condition	Headform Configuration (Azimuth)	Velocity Range (m/s)	Total Impacts	Impacts with harmonic1 <100Hz
American Football	Rear (+180)	3.39-7.69	39	39	Boxing	Rear (+180)	2.45-7.47	15	13
	Right Rear (+135)	3.18-7.47	15	15		Right Rear (+135)	3.58-7.05	12	9
	Right (+90)	3.22-7.26	17	17		Right (+90)	3.80-7.06	12	12
	Right (+90), LOW	2.00-8.46	17	17		Right (+90), LOW	3.44-7.26	12	9
	Right (+90), LOW, OFFSET -5cm	2.32-8.19	15	15		Right (+90), HIGH	3.39-7.47	5	2
	Right (+90), LOW, OFFSET +5cm	2.43-8.45	15	15		Right (+90), LOW, OFFSET +6cm	2.68-6.51	9	9
	Right Front (+45), LOW	2.57-8.46	15	15		Right Front (+45), LOW	2.96-6.05	9	3
	Right Front (+45), HIGH	3.69-7.93	15	15		Right Front (+45), HIGH	1.76-6.51	9	6
	Front (+0), LOW - Facemask	3.80-7.69	15	15		Front (+0), HIGH	3.74-5.91	7	7
	Front (+0), HIGH - Shell	3.86-8.19	15	15	**Table A2-1. Tested ranges for In Vitro Linear Impacts. For some Boxing conditions, harmonic frequencies were too large to apply the harmonic fitting algorithm. These tests were excluded from this analysis.**				

A3. In Vitro Intelligent Mouthguard Co-Registration Scanning Procedure

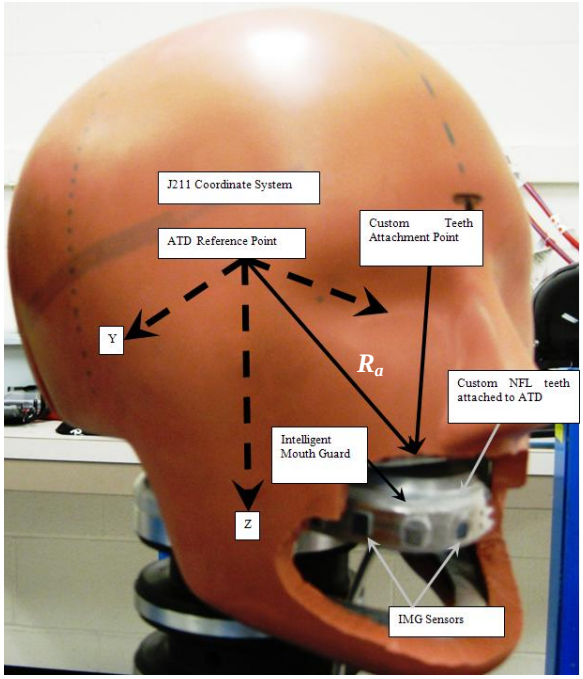

Figure A3-1. Hybrid III ATD with Intelligent Mouthguard on aluminum dentition. The computational algorithm requires knowledge of each sensor location and sensitive axis orientation in J211 coordinate system.

The Intelligent Mouthguard Data Translation Algorithm (DTA) requires accurate knowledge of sensor location and orientation of sensitive axes. The machined aluminum dentition is attached to the ATD on a flat surface X_a-Y_a which is parallel to the X-Y plane of the J211 coordinate system. Vectors X_a and Y_a originate at the attachment point and are parallel to X and Y, respectively.

We determined the dentition attachment point coordinates from manufacturer's drawings and verified by direct measurement using digital calipers. These coordinates define vector $\boldsymbol{R_a}$ in **Figure A3-1**. A translated version of J211 coordinate system can be formed by a normal Z_a to the X_a-Y_a plane at the attachment point and the vectors X_a and Y_a.

Intelligent Mouthguard sensor coordinates relative to the X_a-Y_a-Z_a coordinate system and orientations of the sensor exposed flat surfaces were identified using a laser scanner, see **Figure A3-2**.

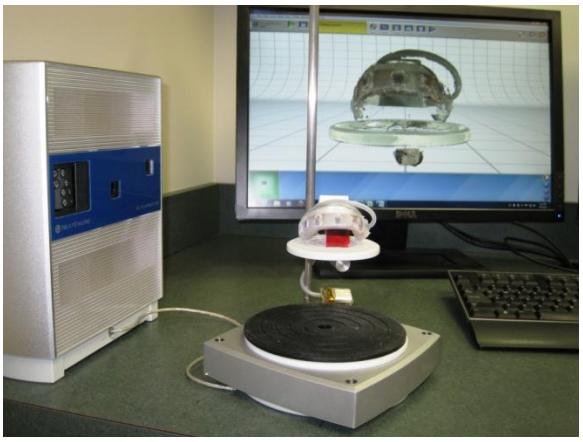

Figure A3-2. Laser Scanning of Intelligent Mouthguard.

Scanning output data contained point clouds of scanned object image in the Scanner Coordinate System. By selecting points of interest, we obtained sensor surface points, attachment point, and X_a, Y_a, Z_a vectors' coordinates in the scanner coordinate system. We converted scanner coordinate system into X_a-Y_a-Z_a coordinate system via a custom Matlab code and using analytical geometry rules. We converted into J211 using simple translation by vector $\boldsymbol{R_a}$ as shown in Table **A3-1**.

Table A3-1. Intelligent Mouthguard sensor locations and sensitive axes orientations in J211 coordinate system.

Position, mm			
	X	Y	Z
G0	81.6	-0.2	68.2
A1	49.0	30.2	63.1
A2	77.3	16.8	67.4
A3	50.2	-30.4	63.7
Sensitive Axis Orientation			
	nx	ny	nz
Gx	0.986	0.005	0.165
Gy	-0.004	1.000	-0.008
Gz	-0.165	0.007	0.986
A1	-0.158	0.007	0.987
A2	-0.645	0.756	-0.109
A3	0.949	0.279	0.150

We estimated location uncertainties at +/- 0.4 mm and sensitive axes orientation uncertainties at +/- 0.6°.

A4. Data Translation Algorithm (DTA)

Intelligent Mouthguard measures three linear accelerations and three orthogonal angular velocities. Sensitive axes are located at known points and orientations. We calculated headform CG rigid body kinematics as a function of time based on sensor measurements. **Figure A4-1** depicts such a free rigid body moving in a global coordinate system ***OXYZ***. Vector R indicates body reference point ***O'*** position relative to point ***O***, vector $\boldsymbol{\omega}$ indicates body angular velocity. There is also a body fixed coordinate system ***O'xyz*** and an arbitrary point ***P*** on the body. Because the body is rigid, point ***P*** position in ***O'xyz*** coordinates does not change. Body movement in ***OZYX*** coordinates is presumed to be a sum of translation of point ***O'*** and rotation around point ***O'***.

Figure A4-1. *An Arbitrary point **P** on a moving rigid body.*

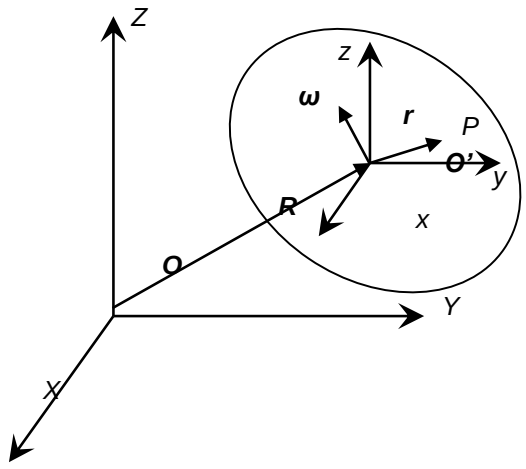

For a point *P* in ***OXYZ*** coordinates:

Position $\boldsymbol{r_P = R + r}$ **(A4-1)**

Velocity $\boldsymbol{v_P = R + r = R + \omega \times r}$ **(A4-2)**

where × denotes vector cross product, $\boldsymbol{r}$ denotes time derivative of $\boldsymbol{r}$

Acceleration $\boldsymbol{a_p = R + \omega \times \ \omega \times r \ + \omega \times r}$ **(A4-3)**

Acceleration of point P is a sum of translational acceleration ***R,*** centripetal acceleration $\boldsymbol{\omega \times \ \omega \times r}$, and tangential acceleration $\boldsymbol{\omega \times r}$**.** For an Intelligent Mouthguard based measurement scheme, not all variables on the right side of equation (**A4-3**) are known. Vector $\boldsymbol{\omega}$ is measured directly by a tri-axial angular rate sensor. Vector $\boldsymbol{r}$ is known and is constant in *O'xyz* for a given point *P*. Vector $\boldsymbol{\omega}$ is a

time derivative of angular velocity, it is not measured directly and has to be derived from $\boldsymbol{\omega}$. Intelligent Mouthguard does not directly measure $\boldsymbol{R}$ which requires detailed analysis of linear acceleration measurements.

Equation (**A4-3**) contains unknown point $\boldsymbol{O'}$ acceleration $\boldsymbol{R}$. By placing point $\boldsymbol{P}$ in the accelerometer locations and applying equation (**A4-3**) components of vector $\boldsymbol{R}$ can be found as a solution of a system of three linear equations with three unknowns for each moment in time. The important condition for the system to have a solution is that no two accelerometers have their sensitive axes parallel to each other. The best numerical accuracy is provided by accelerometer geometrical arrangement when their corresponding sensitive axes are mutually orthogonal. After this step, equation (**A4-3**) can be used again to find acceleration of the arbitrary point $\boldsymbol{P}$ on the moving body.

Effect of Body Rotation

The need to know exact position and orientation of each sensor in global OXYZ coordinate system for the duration of the impact implies the need for correction of sensors' position/orientation as the body rotates during the impact. Although conceptually not difficult, this correction may cause accumulation of numerical errors.

For an accelerometer capable of measuring static acceleration (Earth gravity), change in angular orientation introduces measurement imprecision of up to +/- 1g. However, this imprecision is tolerable, since potentially concussive impacts are characterized by peak amplitude of one to two orders of magnitude higher.

Practical Limitations

This method is applicable under "head as a rigid body" assumption. Considering that each impact signal can be represented by its spectrum, the assumption of rigid body is valid for impact signals with highest frequency component well below frequency of the first mode of the skull. As an example, IMG is not designed to quantify effect of a blast on the body. Although it may be suitable for measuring blast secondary effects, which result in a movement of the head as a rigid body.

A5. Impact Direction and Location

In order to determine impact direction and location (e.g. spatial parameters) on the surface of the head, linear and angular acceleration vectors can be used. In this study, the impact location and direction for Reference (REF) and Intelligent Mouthguard (IMG) data were both computed using head center of gravity (CG) linear acceleration and rigid body calculations of angular acceleration (e.g. temporal parameters).

Our in vitro impacts establishd that headform movement up to peak acceleration (junction between Regions 1 & 2) is on the order of 1-2°. This means the headform does not displace appreciably and the neck develops negligible reaction force during this time. Hence, the headform can be considered a free body at the initial stages of impact, until linear acceleration and angular acceleration reach their peak values. Presuming also that head mass moment of inertia is known about any axis, passing through the head CG, along with the head outer surface geometry, we determined the point on the skull, where the impact force was applied, and the direction of this force.

Theoretical Solution

A force $\boldsymbol{F}$ applied at an arbitrary point on a surface of a free rigid body of mass m and of mass moment of inertia I_m, causes linear acceleration at the body center of gravity $\boldsymbol{a_{cg}}$ and angular acceleration $\boldsymbol{\omega}$. Under this assumption it is possible to determine a line in space, along which the force is acting, and its distance to the body center of gravity. Then the intersection of the force action line with known skull surface geometry identifies the *location* of impact. The *direction* of impact is given by the vector $\boldsymbol{a_{cg}}$. See **Figure A5-1**.

Any vector $\boldsymbol{i}$ can be represented generally as a product of a unit length vector $\boldsymbol{u_i}$,which determines the vector direction, and scalar magnitude *mod*(***i***), which determines the vector length,

$$\boldsymbol{F} = \boldsymbol{u_F} * mod(\boldsymbol{F}); \qquad \boldsymbol{r} = \boldsymbol{u_r} * mod(\boldsymbol{r});$$
$$\boldsymbol{a_{cg}} = \boldsymbol{u_a} * mod(\boldsymbol{a_{cg}}); \qquad \omega = \boldsymbol{u}_\omega * mod(\boldsymbol{\omega});$$

By definition $\boldsymbol{u_F} = \boldsymbol{u_a}$; (**A5-1**)

$\boldsymbol{u_r} \times \boldsymbol{u_a} = \boldsymbol{u}_\omega$; (**A5-2**)

At the same time, $\boldsymbol{F} = m * \boldsymbol{a_{cg}}$ (**A5-3**)

and $\boldsymbol{r} \times \boldsymbol{F} = I_m * \boldsymbol{\omega}$ (**A5-4**)

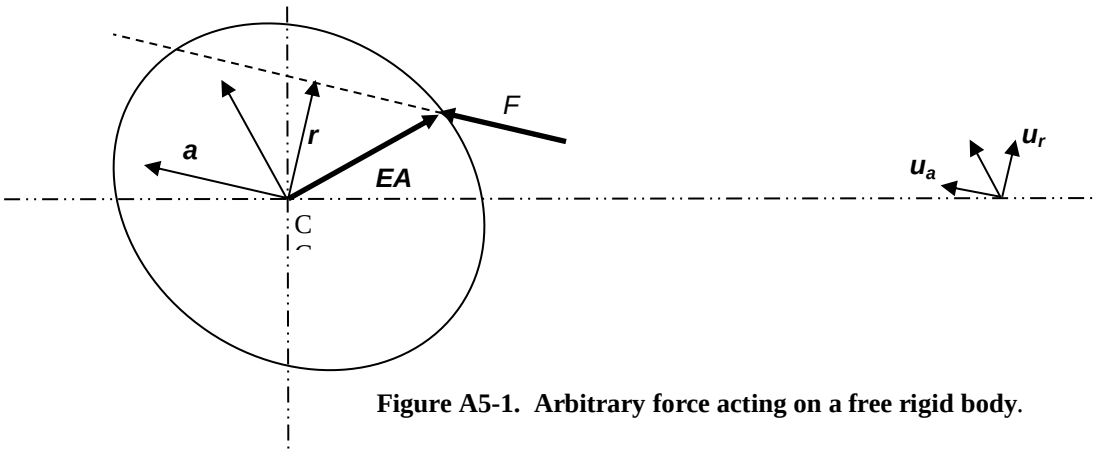

Figure A5-1. Arbitrary force acting on a free rigid body.

Presuming that for a given moment in time, for example the time of peak value, both magnitudes and unit vectors for linear and angular acceleration are known from measurements, the impact direction is known through equation (1), while the impact location can be determined as follows. From equation (2),

$$\boldsymbol{u_r} = \boldsymbol{u_a} \times \boldsymbol{u}_\omega$$

and from equation (**A5-4**) magnitude of vector $\boldsymbol{r}$

$$mod(\boldsymbol{r}) = I_m * mod(\boldsymbol{\omega})/(m * mod(\boldsymbol{a_{cg}})) \quad \textbf{(A5-5)}$$

Therefore, vector $\boldsymbol{r}$ is completely determined, including position of its tip. The location of application of vector $\boldsymbol{F}$ can be found as an intersection of the line defined by the force vector, going through the tip of vector $\boldsymbol{r}$, and the head surface.

Practical limitations

The axis of rotation would be determined through measured vector $\boldsymbol{u}_\omega$. Mass moment of inertia I_m around an arbitrary axis, defined by vector $\boldsymbol{u}_\omega$, is ill defined. A table of $\boldsymbol{I_m}$ values for variety of axes going through head CG would have to be created. The effect of brain being a contained fluid, not a rigid mass, would have to be accounted for in the table. After that the appropriate I_m value can be selected, and coordinates of the tip of vector $\boldsymbol{r}$ can be found from equation (5). In our study, when calculating impact direction and location we assumed mass moment of inertia values from literature (Yoganandan et al., 2009) and calculated Euler Angles (vector *EA*, **Figure A5-1**) to avoid need for meticulous definition of an irregular headform geometrical shape.

The effects of body mass and mass moment of inertia are neglected in this analysis due to assumption that a head can be considered a free body at the initial stages of impact. When this assumption is no longer valid, the location of the impact determined through this method may not be as accurate.

This method is valid for the situation when the head is experiencing rigid body acceleration due to a blow. It indicates location of the force of the blow on the head. For a helmet protected head, a line going from head CG to the predicted impact location point on the head may not go through actual contact area on a helmet due to complex movement of the helmet and due to its protective function. Error in measurements of $\boldsymbol{a_{cg}}$ and $\boldsymbol{\omega}$ would affect the accuracy of impact direction and location prediction, especially for smaller values of acceleration, when the relative error in measurement may increase.

A6. Linear Regression, Accuracy and Precision versus Reference

An ideal instrument has zero inaccuracy, imprecision and perfectly fits a linear model versus Reference. But developing this ideal instrument requires significant time and resources, assuming adequate technologies even exist. A more reasonable approach is to develop an instrument that maximizes linear fit and minimizes inaccuracy and imprecision as much as practically possible.

To qualify an instrument as a single event dosimeter the relationship of instrument data versus Reference data at the time of peak is computed, and linear regression fit of instrument data versus Reference data is quantified. We choose Reference headform CG as the calculation point:

$$IMG_i = mREF_i + b; R^2 \quad \textbf{(A6-1)}$$

Where REF_i is the X, Y, or Z component Reference output at time of peak
IMG_i is the X, Y, or Z component Intelligent Mouthguard output at time of peak
m is the slope of the fitted line
b is the y-intercept of the fitted line

R^2 is the coefficient of determination, which quantifies how closely the data fit the linear model.

We quantify accuracy and precision, in kinematic or spatial units of interest, at time of peak CG acceleration as the average (δ_{pk}) and standard deviation (σ_{pk}) of differences between peak Intelligent Mouthguard and Reference XYZ primary impact components with peak linear acceleration greater than 15g. This precision is grouped into three bins *B* by first harmonic frequency (bin1 <50Hz, bin2 51-70Hz, bin3 71-100Hz):

$$\delta_{pk} = average(REF_i - IMG_i) \quad \textbf{(A6-2)}$$

$$\sigma_{pk} = \sqrt{\frac{\sum_{i=1}^{n} REF_i - IMG_i\ ^2}{n-1}} \quad \textbf{(A6-3)}$$

Where δ_{pk} is the average error at time of peak for each frequency bin
σ_{pk} is the precision at time of peak for each frequency bin
n is the number of points in each frequency bin

We also calculate Intelligent Mouthguard average temporal accuracy (δ) and precision (σ) for each set of XYZ component CG linear acceleration and angular acceleration time traces with peak linear acceleration greater than 15g in a primary impact direction. These parameters are calculated separately in Region 1, Region 2 and Region 3 (**Figure 2**) and grouped by harmonic frequency bin as follows:

(1) Separate test-specific time traces into frequency bins.
(2) Divide the time traces of all XYZ components in a given test into Region 1, Region 2 and Region 3.
(3) For a given test, and each time trace Region, use equation **A6-2**, but substitute all values in the time traces of Reference and Intelligent Mouthguard for the XYZ component of interest (linear CG and angular acceleration). This is the temporal accuracy in each Region of one test.
(4) For a given test, and each time trace Region, use equation **A6-3**, but substitute all values in the time traces of Reference and Intelligent Mouthguard for the XYZ component of interest (linear CG and angular acceleration). This is the precision in each Region of one test.
(5) Calculate the average temporal accuracy (δ) of all tests, separated by Regions and assigned frequency bins, by summing individual temporal accuracies and dividing by number of tests in each bin.
(6) Calculate the average temporal precision (σ) of all tests, separated by Regions and assigned frequency bins, by summing individual temporal precisions and dividing by number of tests in each bin.

REFERENCES

Aksu, A., (2013). Benchtop Validation of Intelligent Mouthguard. Cleveland State University.

Arbogast, K. B., McGinley, A. D., Master, C. L., Grady, M. F., Robinson, R. L., Zonfrillo, M. R., (2013). Cognitive Rest and School-Based Recommendations Following Pediatric Concussion: The Need for Primary Care Support Tools. Clin.Pediatr.(Phila).

Beckwith, J. G., Chu, J. J., Greenwald, R. M., (2007). Validation of a noninvasive system for measuring head acceleration for use during boxing competition. J.Appl.Biomech. 23**,** 238-244.

Beckwith, J. G., Greenwald, R. M., Chu, J. J., (2012). Measuring head kinematics in football: correlation between the head impact telemetry system and Hybrid III headform. Ann.Biomed.Eng 40**,** 237-248.

Beckwith, J. G., Greenwald, R. M., Chu, J. J., Crisco, J. J., Rowson, S., Duma, S. M., Broglio, S. P., McAllister, T. W., Guskiewicz, K. M., Mihalik, J. P., Anderson, S., Schnebel, B., Brolinson, P. G., Collins, M. W., (2013a). Head Impact Exposure Sustained by Football Players on Days of Diagnosed Concussion. Med.Sci.Sports Exerc. 45**,** 737-746.

Beckwith, J. G., Greenwald, R. M., Chu, J. J., Crisco, J. J., Rowson, S., Duma, S. M., Broglio, S. P., McAllister, T. W., Guskiewicz, K. M., Mihalik, J. P., Anderson, S., Schnebel, B., Brolinson, P. G., Collins, M. W., (2013b). Timing of Concussion Diagnosis Is Related to Head Impact Exposure Prior to Injury. Med.Sci.Sports Exerc. 45**,** 747-754.

Broglio, S. P., Swartz, E. E., Crisco, J. J., Cantu, R. C., (2011). In vivo biomechanical measurements of a football player's C6 spine fracture. N.Engl.J.Med. 365**,** 279-281.

Camarillo, D. B., Shull, P. B., Mattson, J., Shultz, R., Garza, D., (2013). An instrumented mouthguard for measuring linear and angular head impact kinematics in American football. Ann.Biomed.Eng 41**,** 1939-1949.

Cantu, R. C., (1998). Second-impact syndrome. Clin.Sports Med. 17**,** 37-44.

Centers for Disease Control, (2011). Nonfatal sports and recreation related traumatic brain injuries among children and adolescents treated in emergency departments in the United States, 2001-2009. United States Centers for Disease Control and Prevention-Morbidity and Mortality Weekly Report (MMWR), pp. 1337-1342.

Crisco, J. J., Fiore, R., Beckwith, J. G., Chu, J. J., Brolinson, P. G., Duma, S., McAllister, T. W., Duhaime, A. C., Greenwald, R. M., (2010). Frequency and location of head impact exposures in individual collegiate football players. J Athl.Train. 45**,** 549-559.

Daneshvar, D. H., Riley, D. O., Nowinski, C. J., McKee, A. C., Stern, R. A., Cantu, R. C., (2011). Long-term consequences: effects on normal development profile after concussion. Phys.Med.Rehabil.Clin.N.Am. 22**,** 683-700, ix.

Daniel, R. W., Rowson, S., Duma, S. M., (2012). Head impact exposure in youth football. Ann.Biomed.Eng 40**,** 976-981.

Duma, S. M., Manoogian, S. J., Bussone, W. R., Brolinson, P. G., Goforth, M. W., Donnenwerth, J. J., Greenwald, R. M., Chu, J. J., Crisco, J. J., (2005). Analysis of real-time head accelerations in collegiate football players. Clin.J.Sport Med. 15**,** 3-8.

Duma, S. M., Rowson, S., (2011). Past, present, and future of head injury research. Exerc.Sport Sci.Rev. 39**,** 2-3.

Funk, J. R., Rowson, S., Daniel, R. W., Duma, S. M., (2012). Validation of concussion risk curves for collegiate football players derived from HITS data. Ann.Biomed.Eng 40**,** 79-89.

Greenwald, R. M., Gwin, J. T., Chu, J. J., Crisco, J. J., (2008). Head impact severity measures for evaluating mild traumatic brain injury risk exposure. Neurosurgery 62**,** 789-798.

Guskiewicz, K. M., Marshall, S. W., Bailes, J., McCrea, M., Cantu, R. C., Randolph, C., Jordan, B. D., (2005). Association between recurrent concussion and late-life cognitive impairment in retired professional football players. Neurosurgery 57**,** 719-726.

Guskiewicz, K. M., Marshall, S. W., Bailes, J., McCrea, M., Harding, H. P., Jr., Matthews, A., Mihalik, J. R., Cantu, R. C., (2007a). Recurrent concussion and risk of depression in retired professional football players. Med.Sci.Sports Exerc. 39**,** 903-909.

Guskiewicz, K. M., Mihalik, J. P., (2010). Biomechanics of Sport Concussion: Quest for the Elusive Injury Threshold. Exerc.Sport Sci.Rev.

Guskiewicz, K. M., Mihalik, J. P., Shankar, V., Marshall, S. W., Crowell, D. H., Oliaro, S. M., Ciocca, M. F., Hooker, D. N., (2007b). Measurement of head impacts in collegiate football players: relationship between head impact biomechanics and acute clinical outcome after concussion. Neurosurgery 61**,** 1244-1252.

Hakansson, B., Brandt, A., Carlsson, P., Tjellstrom, A., (1994). Resonance frequencies of the human skull in vivo. J.Acoust.Soc.Am. 95**,** 1474-1481.

Institute of Medicine and National Research Council, (2014). Sports-Related Concussions in Youth: Improving the Science, Changing the Culture. In: Graham, R., Rivara, FP., Ford, MA., Spicer, CM. (Eds.), The National Academies Press, Washington, DC.

Jadischke, R., Viano, D. C., Dau, N., King, A. I., McCarthy, J., (2013). On the accuracy of the Head Impact Telemetry (HIT) System used in football helmets. J.Biomech. 46**,** 2310-2315.

Jordan, B. D., (2000). Chronic traumatic brain injury associated with boxing. Semin.Neurol. 20**,** 179-185.

Kang, Y. S., Moorhouse, K., Bolte, J. H., (2011). Measurement of six degrees of freedom head kinematics in impact conditions employing six accelerometers and three angular rate sensors (6aomega configuration). J.Biomech.Eng 133**,** 111007.

Mansell, J. L., Tierney, R. T., Higgins, M., McDevitt, J., Toone, N., Glutting, J., (2010). Concussive signs and symptoms following head impacts in collegiate athletes. Brain Inj. 24**,** 1070-1074.

McAllister, T. W., Ford, J. C., Flashman, L. A., Maerlender, A., Greenwald, R. M., Beckwith, J. G., Bolander, R. P., Tosteson, T. D., Turco, J. H., Raman, R., Jain, S., (2014). Effect of head impacts on diffusivity measures in a cohort of collegiate contact sport athletes. Neurology 82**,** 63-69.

McCrea, M., Hammeke, T., Olsen, G., Leo, P., Guskiewicz, K., (2004). Unreported concussion in high school football players: implications for prevention. Clin.J Sport Med. 14**,** 13-17.

McElhaney, J. H., (2005). In search of head injury criteria. Stapp.Car.Crash.J. 49**,** v-xvi.

McKee, A. C., Cantu, R. C., Nowinski, C. J., Hedley-Whyte, E. T., Gavett, B. E., Budson, A. E., Santini, V. E., Lee, H. S., Kubilus, C. A., Stern, R. A., (2009). Chronic traumatic encephalopathy in athletes: progressive tauopathy after repetitive head injury. J.Neuropathol.Exp.Neurol. 68**,** 709-735.

Mihalik, J. P., Blackburn, J. T., Greenwald, R. M., Cantu, R. C., Marshall, S. W., Guskiewicz, K. M., (2010). Collision type and player anticipation affect head impact severity among youth ice hockey players. Pediatrics 125**,** e1394-e1401.

National Operating Committee on Standards for Athletic Equipment (NOCSAE), (2006). Standard Linear Impactor Test Method and Equipment Used in Evaluating the Performance Characteristics of Protective Headgear and Face Guards. Overland Park, KS, pp. 1-6.

Omalu, B. I., DeKosky, S. T., Minster, R. L., Kamboh, M. I., Hamilton, R. L., Wecht, C. H., (2005). Chronic traumatic encephalopathy in a National Football League player. Neurosurgery 57**,** 128-134.

Omalu, B. I., Fitzsimmons, R. P., Hammers, J., Bailes, J., (2010). Chronic traumatic encephalopathy in a professional American wrestler. J.Forensic Nurs. 6**,** 130-136.

Ozturk, C., (2013). Method for Determination of Kinematic Sensor Position and Orientation from Magnetic Resonance Images. Cleveland State University.

Padgaonkar, A. J., Krieger, K. W., King, A. I., (1975). Measurement of angular acceleration of a rigid body using linear accelerometers. Journal of Applied Mechanics-Transactions of the ASME 552-556.

Plassman, B. L., Havlik, R. J., Steffens, D. C., Helms, M. J., Newman, T. N., Drosdick, D., Phillips, C., Gau, B. A., Welsh-Bohmer, K. A., Burke, J. R., Guralnik, J. M., Breitner, J. C., (2000). Documented head injury in early adulthood and risk of Alzheimer's disease and other dementias. Neurology 55**,** 1158-1166.

Rowson, S., Beckwith, J. G., Chu, J. J., Leonard, D. S., Greenwald, R. M., Duma, S. M., (2011). A six

degree of freedom head acceleration measurement device for use in football. J Appl.Biomech. 27**,** 8-14.

Rowson, S., Brolinson, G., Goforth, M., Dietter, D., Duma, S., (2009). Linear and angular head acceleration measurements in collegiate football. J Biomech.Eng 131**,** 061016.

Rowson, S., Duma, S. M., (2011). Development of the STAR evaluation system for football helmets: integrating player head impact exposure and risk of concussion. Ann.Biomed.Eng 39**,** 2130-2140.

Siegmund, G. P., Guskiewicz, K., Marshall, S. W., DeMarco, A. L., Bonin, S. J., (2014). Validation of Wearable Sensors for Football Head Impacts., Boston, MA, USA.

Society of Automotive Engineers, (2003). SAE Recommended Practice: Instrumentation for Impact Test-Part 1-Electronic Instrumentation-SAE J211/1 Dec03. Society of Automotive Engineers, Warrendale, Pennsylvania, USA.

Society of Automotive Engineers, (1994). SAE Information Report: Sign Convention for Vehicle Crash Testing-SAE J1733 Dec94. Society of Automotive Engineers, Warrendale, Pennsylvania, USA.

Stapp, J. P., (1978). Closing Remarks., Ann Arbor, MI.

Wonnacott, M., Withnall, C., (2010). Development of an Articulating Mandible Headform Having Force Sensing Temporomandibular Joints. Society of Automotive Engineers.

Yoganandan, N., Pintar, F. A., Zhang, J., Baisden, J. L., (2009). Physical properties of the human head: mass, center of gravity and moment of inertia. J.Biomech. 42**,** 1177-1192.